M.I. GORBUNOV, M.V. KOVTANETS, O.V. SERHIIENKO,
T.M. KOVTANETS, V.S. NOZHENKO

PREDICTION OF TRACTIVE AND DYNAMIC PERFORMANCE OF LOCOMOTIVES BY SIMULATION MODELING

Monograph

2021

MINISTRY OF EDUCATION AND SCIENCE OF UKRAINE
VOLODYMYR DAHL EAST UKRAINIAN NATIONAL UNIVERSITY

M. I. GORBUNOV, M. V. KOVTANETS,
O. V. SERHIIENKO, T. M. KOVTANETS, V. S. NOZHENKO

PREDICTION OF TRACTIVE AND DYNAMIC PERFORMANCE OF LOCOMOTIVES BY SIMULATION MODELING

Monograph

Severodonetsk 2021

UDC 625.032.3
G 671

This monograph is recommended for printing by the Science Council Volodymyr Dahl East Ukrainian National University (Protocol № 4 from 26 november 2021 year)

Reviewers:

Fomin O.V., Ph.D., Professor, Professor of Wagons and Carriage Management Department, State University of Infrastructure and Technology;

Domin Yu.V., Ph.D., Professor, Professor of Railway and Road Transport, Lift and Care Systems Department, Volodymyr Dahl East Ukrainian National University.

Gorbunov M.I., Kovtanets M.V., Serhiienko O.V., Kovtanets T.M., Nozhenko V.S.

Prediction of tractive and dynamic performance of locomotives by simulation modeling: Monograph / M.I. Gorbunov, M.V. Kovtanets, O.V. Serhiienko, T.M. Kovtanets, V.S. Nozhenko. – Severodonetsk: EUNU, 2021. – 94 p.

ISBN 978-617-11-0219-4

The monograph considers the issues of assessing the traction and dynamic qualities of locomotives based on the methods of simulation modeling of the processes of frictional interaction between the wheel and the rail, the characteristics of the suspension elements and the movement of the rail vehicle.

УДК 625.032.3
Г 671

ISBN 978-617-11-0219-4

TABLE OF CONTENTS

1 RAIL VEHICLE MOTION SIMULATION MODELING

In the process of the rolling stock development, one needs to take into account the influence of various design and dynamic parameters of the vehicle, which cannot be experimentally obtained due to the extremely high labor intensity and multivariate field tests. Simulation modeling based on reliable experimental data allows identifying these dependencies and making sure the search for circuit solutions goes in the right way.

Simulation is defined as the process of constructing a model of a real system and setting up experiments on that model in order to understand the behavior of the system and to use the model to predict its future behavior. Simulation methods are used to analyze the economic systems, in queuing problems, environmental, physics, technology and other areas [79]. This method appears to be particularly widespread because, unlike other modeling methods such as physical, analog, or based on the theory of similarity and dimensions [35], the computer-assisted simulation allows studying the behavior of complex systems for which one cannot give a complete mathematical formulation of how they work, taking into account all known system connections and their random nature.

In the course of modeling, a number of problems need to be solved. The first circle of problems is associated with the model construction methodology: one needs to choose the dimension of the model and its variables, identify the model, and select the type of disturbance from the path. The second circle is associated with the provision of a rational technology for working with the model. This includes: the choice of the method for presenting the initial data and calculation results in the form familiar to the researcher, the methods of interaction between the researcher and the computer, etc. Note that the correct solution to the second circle of problems largely contributes to the ability to build an adequate model.

According to the experience of numerous researchers, the adequacy of the model does not always increase with the increasing dimension. This is due to the limited capacity of identifying models with a large number of interrelated parameters, as well as the effect of the error accumulation in determining the said parameters. The solution to this problem is dictated by the logic of the research and the availability of experimental data.

On the basis of these provisions, a simulation model of the rail vehicle motion was developed in this monograph, the block diagram of which is set forth in Fig. 1.

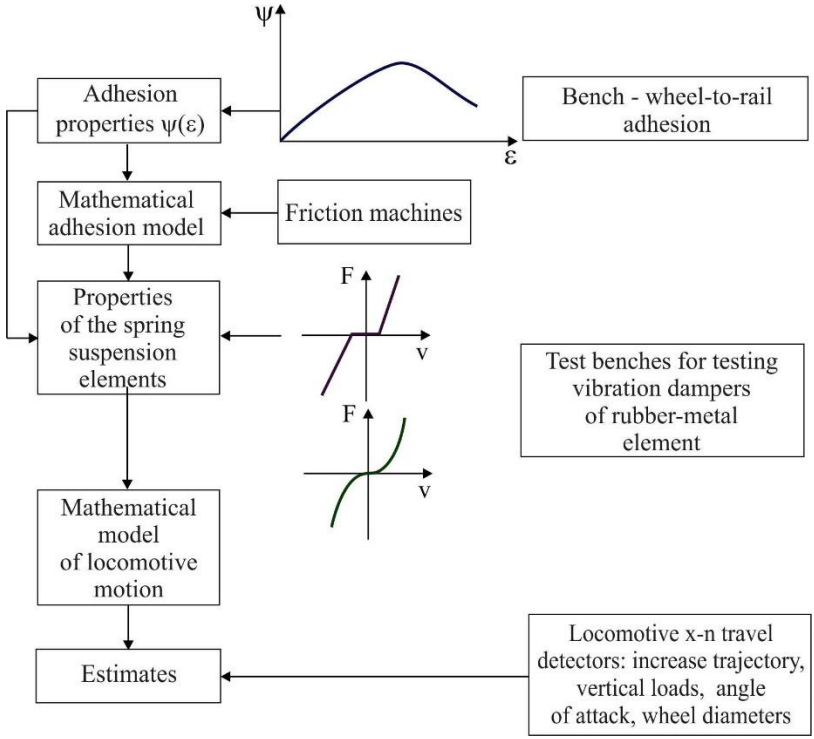

Fig. 1. Simulation model block diagram

2 REVIEW OF METHODS FOR ACCOUNTING THE ADHESION FORCES IN SOLVING THE TRACTION AND DYNAMIC PROBLEMS OF THE RAILWAY VEHICLE MOTION

The forces arising out of the interaction between the wheel and the rail have a considerable effect on the dynamic behavior of the vehicle [52, 65]. In turn, its dynamic properties have a considerable impact on the adhesion forces. This implies the importance of an adequate modeling of the wheel-to-rail adhesion process in mathematical models of the locomotive motion in order to study their traction and dynamic performance.

In the dynamic models studying the movement of rail vehicles there is no unity in terms of using certain mathematical models of the wheel-to-rail adhesion.

Fig. 2 shows the classification of these models developed in [16, 21, 45], which divides the adhesion models into theoretical and experimental.

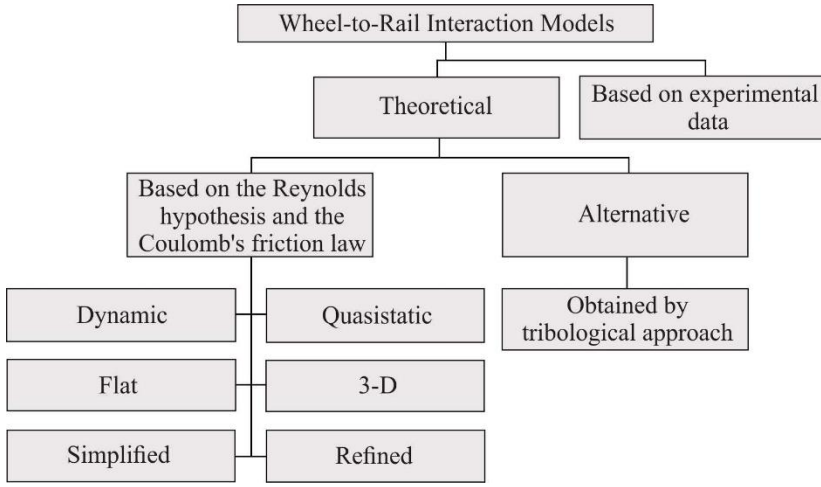

Fig. 2. Classification of wheel-to-rail interaction models

Experimental models are used in works dealing with the study of the tractive force generated by a locomotive, taking into account the dynamic impact. These models can be the result of a specially conducted experiment in order to implement them on a locomotive [64] or on a test bench [70, 81].

To this end, an empirical relationship was established in [64] between the adhesion coefficient and the coefficient of sliding friction, the speed of the locomotive (V, km/h), and the relative sliding (V_{sl}, %) for an electric locomotive.

$$\psi = -0{,}16297 + 1{,}49473f + 0{,}09387V_{sl} - 0{,}0014V - 0{,}155fV_{sl} - 0{,}00539fV - 0{,}00013V_{sl}V - 1{,}056f^2 - 0{,}015V_{sl}^2 + 0{,}000025V^2.$$

This formula was obtained for a specific locomotive and cannot be used in the study of other types of locomotives, especially the newly developed ones. Furthermore, the profiles of wheels and rails and their mutual orientation are not taken into account here.

In some cases [62], experimental adhesion models are the result of generalization and the analysis of a number of experimental data obtained from various sources.

In [51], as the results of numerous experimental studies (Fig. 3) when building a mathematical model of the motion, the approximating dependence $\psi_{ad} = f(\varepsilon_{sl})$ of the locomotive's bogie. The disadvantage of this approach is that an average characteristic is used, regardless of frictional conditions, travel speed, vertical load, lateral sliding, wheel and rail profiles, vehicle design, etc.

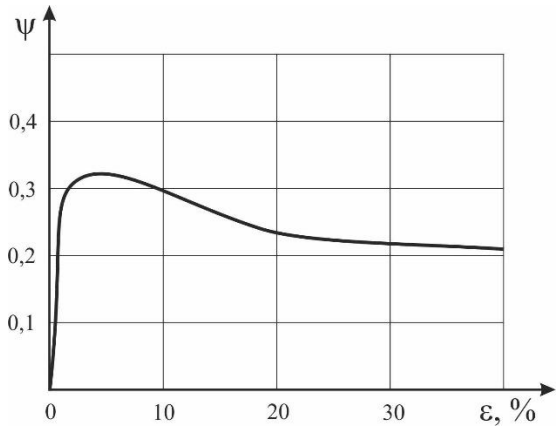

Fig. 3. Adhesion behavior model built according to [51]

Based on the results of numerous experimental studies, [51] presents the dependence $\psi_{ad} = f(\varepsilon_{sl})$ (Fig. 3), which is used to build a mathematical model of the locomotive bogie's movement.

Taking into account the shortcomings of experimental adhesion models, theoretical models of adhesion are often used in works dealing with modeling the dynamics of the rail vehicle's motion. Most of these are based on Osborne Reynolds' assumption that the contact zone consists of an adhesion zone where the true sliding is $\vec{S} = 0$, and the sliding zone, where $\vec{S} > 0$. The second feature of this theory is the use of the Coulomb relation as the law of friction, which can be mathematically written as

$$|\vec{\tau}| \leq f_\sigma \ at \ |\vec{S}| = 0,$$

$$\vec{\tau} = -f\sigma \frac{\vec{S}}{|\vec{S}|}, \; at \; |\vec{S}| > 0,$$

where τ - tangential stresses;

δ- normal stresses;

and f is the coefficient of sliding friction.

Let us consider the theoretical models of adhesion most frequently used in the studies of the vehicle's dynamics.

One of the first and extensively used to date is the Carter's theoretical model [83], which is flat in an exact formulation, according to which the longitudinal forces of the creep are proportional to the relative sliding.

$$F_x = -k\varepsilon_x, \quad (1)$$

where F_X is the projection of the adhesion force onto the coordinate axis directed along the railway track in the horizontal plane;

ε_X is the dimensionless relative sliding, which is the ratio of the mutual travels of the contacting surfaces in the longitudinal direction to the total translational travel;

k is the constant called the creep force factor.

Carter [16] considered only the longitudinal creep force, but to solve the problem of the vehicle's motion, one needs to determine its transverse component as well. It is usually assumed that similar ratios apply in the transverse direction.

For steel wheels and rails [16]

$$k = A\sqrt{RlP(1-\sqrt{1-\tau})},$$

where A is the matching coefficient;

R - the radius of the wheel;

l - the equivalent length of the contact pad;

P - the vertical load from the wheel on the rail;

τ- the ratio of the tangential force F to the greatest adhesion force equal to $P\mu$ (μ - coefficient of friction). For l=25 mm and τ=0.25

$$k = 2530\sqrt{RP},$$

P [kH], R [m].

In the same formulation (that is, the flat one), the contact problem of the rolling and sliding was considered in the works of Fromm [86], V.I. Mossakovsky [57], etc. For example, in [57], the expression for the longitudinal tangential force F_X was obtained in the form of

$$F_x = 2\sqrt{\frac{P' RG\pi}{\chi+1}}\frac{\delta_c}{v} + \frac{\pi GRl_1}{(\chi+1)f_0}\left(\frac{\delta_c}{v}\right)^2,$$

where δ_c – the sliding speed, defined as the speed of the mutual travel of the wheel-to-rail contact surfaces;

v is the speed of the forward motion of the wheel;

f_0 – the coefficient of sliding friction;

χ - the ratio that depends on Poisson's ratio;

P' is the load from the wheel on the rail per unit length of the contact strip, $P' = P/l_1$; l_1 - the length of the contact strip. The ratio δ_c / v is the relative sliding defined by ε.

The main disadvantage of the flat models is that only the longitudinal component of the sliding vector is taken into account, and this does not allow determining the transverse component of the adhesion force and the resistance to the relative rotation (spin).

Spatial models are free from this disadvantage. They take into account not only the longitudinal relative sliding, but the transverse one as well, and the sliding that occurs during the mutual rotations of the contacting bodies relative to the axis being normal to the contact area.

The linear Kalker theory [40, 87] is widely used in problems of railway vehicle dynamics [40, 87]. It was obtained by solving the spatial contact problem of the theory of elasticity under the assumption that for vanishingly small wheel sliding on the rail, the projections of the adhesion force and the torque are represented by the linear functions ε_x, ε_y and ξ.

The solution appears to be as follows:

$$F_x = c^2 G C_{11} \varepsilon_x;$$
$$F_y = c^2 G C_{22} \varepsilon_y + c^3 C_{23} G \xi;$$
$$F_z = -c^3 G C_{23} \varepsilon_y + c^3 C_{33} G \xi,$$

where $c = \sqrt{ab}$; a and b – the semi-axes of an elliptical contact area;

G - Young's modulus.

This can only be used to study motion in coasting mode due to the assumptions made in their derivation and cannot be used to determine the adhesion force when the traction (braking) moment is generated by the locomotive's wheel, since these modes cause significant sliding.

The adhesion models based on solving the spatial problem of the interaction of two bodies during rolling with sliding in an exact formulation have become widespread recently. However, their direct application in solving the differential equations of the locomotive motion, even with the use of modern computers, is difficult due to the prohibitive cost of machine time. Therefore, in problems of the

dynamics of rail vehicles, approximate analytical expressions are usually used, obtained by approximating the results of a computer experiment [16, 19, 52, 73, etc.].

As an example of such an approach, we can cite the formulas obtained from the data of a computer experiment [52, 73], and the numerical solution of the spatial contact problem of the theory of elasticity on the stationary rolling of the wheel on the rail [4]:

$$F = -T_n \varepsilon \left[\left(T_n \varepsilon / \mu P \right)^m + 1 \right]^{\left(-\frac{1}{m} \right)}, \qquad (2)$$

where T_n - coefficient that depends on n of the additional factors affecting the creep force, $T_n \prod_{i=1} T_i$, for example, T_1 takes into account the change in the vertical load from the wheel on the rail, T_2 is the rolling radius of the wheel, T_3 is the position of the contact spot on the rail surface, T_4 is the rolling of the wheel, T_5 is the wear of the rails, etc.;

μ - coefficient of friction;

parameter *m is* usually used equal to 4.

Wherein

$$T_1 = 235P - 2{,}4P^2 + 0{,}01P^3 \text{ [kN]}$$

$$T_2 = 1400\sqrt{PR}, \text{ F and P [kN], R [m]}$$

$$T_3 = T_2(3.5 + 0.5\text{th}(4.5 - 0.5|yc|))/4 = 350(3.5 + 0.5\text{th}(4.5 - 0.5|yc|))\sqrt{PR},$$

where F is the wheel-to-rail adhesion force, [kN];

P - the vertical load from the wheel on the rail, [kN];

R is the radius of the wheel, [m];

$|yc|$ - the modulus of travel of the contact spot from the plane of symmetry of the rail, [mm];

$$T_4 = T_3(1 + 0{,}8\Delta R); \qquad T_5 = T_4\left[1 - (0{,}05 + 0{,}08\Delta R)\right],$$

where ΔR - wheel tire wear [mm];

Formulas similar to (2) were used by other authors, but the value of m ranged from 1 to 2. For example, Levy takes m=1 [90], Charter - m=2 [91].

In [16], variants of the theory of interaction of two bodies are presented in an exact formulation and expressions suggested by Kalker that approximate the dependence of the adhesion force

$$\left|\frac{N}{F_x}\right|^n = \left|\frac{\varepsilon}{\varepsilon_x f}\right|^n + \left|\frac{N}{abGC_{11}\varepsilon_x}\right|^n;$$

$$\left|\frac{N}{F_y}\right|^n = \left|\frac{\varepsilon}{\varepsilon_y f}\right|^n + \left|\frac{N}{abGC_{22}\varepsilon_y}\right|,^n$$

where N is the total normal force;

a – the semi-axis of the contact ellipse in the longitudinal direction;

b – the semi-axis of the contact ellipse in the transverse direction;

f is the coefficient of friction.

In [90], the value of n was taken equal to 1, and in [84], n=2.

Let us compare the calculation results obtained for all of the above theoretical models of adhesion with experimental data.

Generally, theoretical models of adhesion provide the following results [45]:

1) with an increase in sliding from zero to ε_{kr} the adhesion coefficient increases, and after exceeding ε_{kr} - does not change;
2) the calculated value ε_{kr} is within 0.1-0.5%;
3) with the deterioration of frictional conditions of the contact, the critical sliding shifts towards the smaller sliding;
4) changes in the vertical load on the wheel and the speed of the locomotive do not affect the coefficient of adhesion.

The analysis of experimental works dealing with the problem of adhesion [45, 53, 65, 74, 92, 95, 63, 58, etc.] allows us to formulate the general laws of the process of the wheel-to-rail adhesion:

1. adhesion is based on the external friction forces;
2. the adhesion force cannot be generated without the relative sliding of the wheel relative to the rail;
3. the adhesion behavior has a more or less pronounced maximum;
4. the locomotive speed in the range of 20-120 km/h has little effect on adhesion (if the experiment is carried out in ideal laboratory conditions). The apparent decrease in the adhesion coefficient with an increase in the speed of motion is explained by the dynamic nature of the interaction between the wheels and the rails. With an increase in the speed of motion, the critical sliding decreases;
5. the critical sliding corresponding to the maximum on the adhesion behavior, depending on the frictional conditions of contact, varies greatly (ranging from 2 to 15 and even 20%);
6. with the deterioration of the frictional conditions of contact, the maximum on the adhesion behavior decreases, and the maximum itself shifts to the zone of the larger slidings;

7. the friction coefficient decreases with the increase of the normal wheel load.

Therefore, the results of experimental and theoretical studies of adhesion differ both quantitatively (Fig. 4) and qualitatively. While theoretical models and the results of experimental work are close when it comes to small slidings (without the application of the traction moment), the difference becomes significant with a further increase in the sliding values. If the wheel generates the traction (braking) torque, i.e. in the presence of a significant sliding, the use of theoretical models of adhesion that are based on the Reynolds hypothesis and Coulomb's law of friction, will lead to significant errors in the calculations while modeling the locomotive motion.

Therefore, some authors, when constructing theoretical models of the adhesion process, used the latest advances in the science of friction - tribology [45, 89, 59]. This group of theoretical models of adhesion is referred to as the alternative one [45]. Models of the alternative group, with the exception of [89] in [93], were not used in the rail vehicle motion problems, since they do not take into account the dynamic nature of the wheel-to-rail interaction and do not make it possible to construct the adhesion behavior - the main one for describing the rolling process of the bodies of revolution. In alternative models, no dependence of the adhesion coefficient (adhesion force) on the sliding has been obtained.

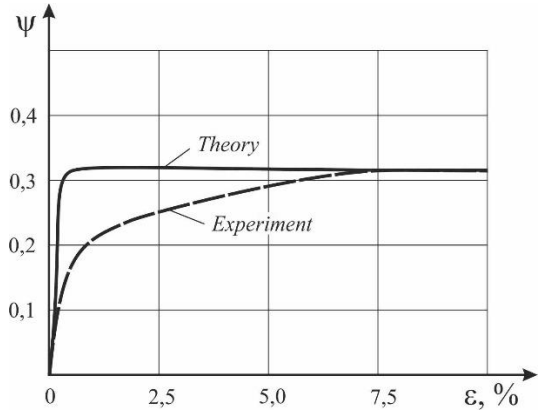

Fig. 4. Adhesion behavior model built according to [4] and [92]

Based on the results of the above analysis, one can conclude that the mathematical model of the adhesion of the locomotive's wheel to the rail and the model of the locomotive as a whole should be built taking into account the simulation, i.e. the experimental data.

3 MODELING THE LOCOMOTIVE WHEEL TO THE RAIL ADHESION PROCESS

3.1. Study of the wheel-to-rail adhesion on a test bench

To determine the experimental dependencies of the adhesion coefficient of a wheel to the rail on the action of various factors, such as the stiffness of the rail, the angle of attack, the vertical load in contact, the material and condition of the wheel and rail surface, dynamic forces in contact, etc., the author has upgraded the VMSI bench, a mechanism for vertical and horizontal dynamic loading of a wheel, a device to simulate a change in the rail stiffness, a mechanism for turning the wheel axis in plan have been manufactured and set up on a bench assembly.

The experimental setup is designed in such a way that it makes it possible to exclude the influence of side factors observed when testing the full-scale locomotives on the adhesion process and to study the adhesion coefficient in conditions of contact close to the real ones, at various modes of movement.

Fig. 5 is a schematic representation of the proposed bench, the general view; Fig. 6 - the same, top view.

The bench comprises a drive installed on foundation 1, containing an electric motor 2, a flywheel 3, a hydraulic torque converter 4, connected by a drive shaft with a reversible gearbox 5. The latter is mounted on rubber supports with the ability to move and is coupled by means of coupling 6 and wheel 7. Wheel 7 is mounted on an axle in the axle box unit 8, attached to the upper part of the frame 10 of the bench by means of spring suspension elements 9. The upper part of the frame 10 of the bench is mounted on the bottom part 11 of the frame with the possibility of vertical movement. On the base 12 of the bench, the main 13 and auxiliary 14 support rollers, as well as two horizontal thrust rollers 15, are installed. Lift mechanisms 16 and 17, installed on the base bracket 12, allow to adjust the distance between the main support rollers 13 and the contact point of the wheel 7 with the rail 18 and between the thrust rollers 15 and the point of contact of the wheels with the rail. The rail 18 is mounted on rollers 13 and 14, and the wheel 7, in turn, rests on it. In the upper part of the frame 10 of the bench, there are mechanisms 19 for vertical loading of the wheel (hydraulic jack) and a mechanism 20 for vertical dynamic loading of the wheel 7. Mechanism 21 of the horizontal dynamic loading of the axle box unit is installed in the axle box unit 8 and is connected to the axle of the wheel 7. The bench is equipped with a mechanism for longitudinal rail loading, designed as an electromagnetic brake, there are stops 23 that contact the protrusions 24, tractive force sensors are installed. The bench has

wheel speed sensors 7 and a rail sensor 18, hydraulic and pneumatic control sensors of the bench, the amplifying and the recording units (not shown).

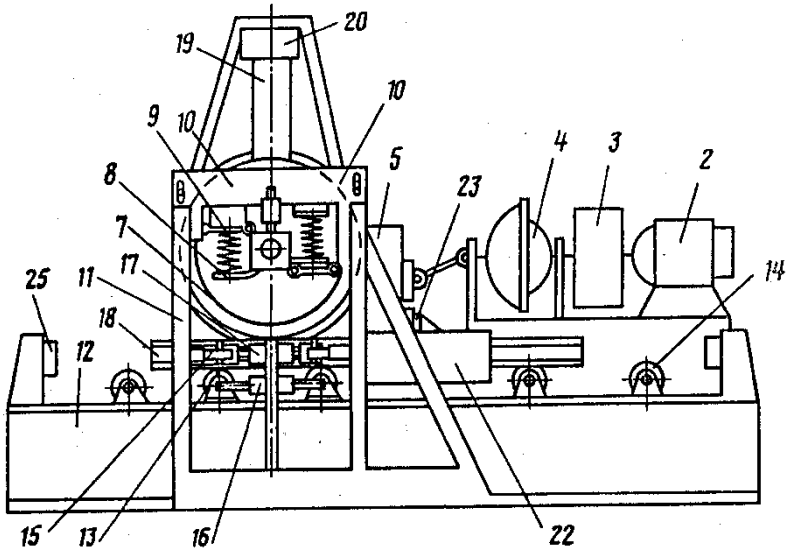

Fig. 5. Wheel-to-rail adhesion test bench (side view)

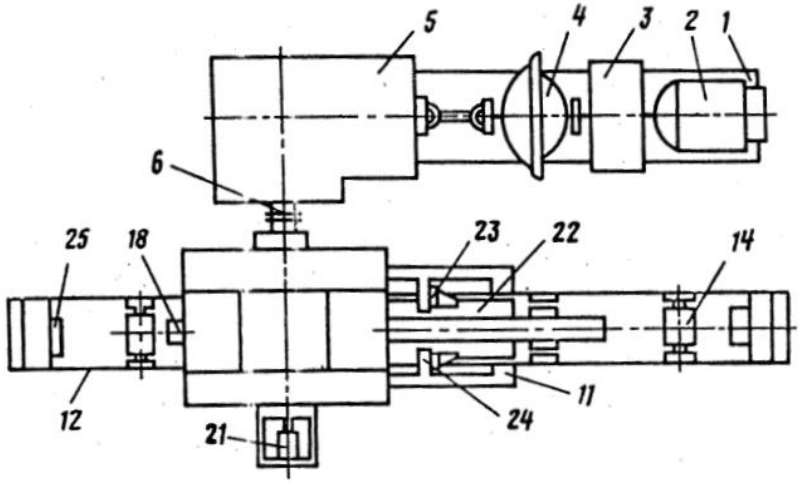

Fig. 6. Wheel-to-rail adhesion test bench (top view)

On the base 12 of the bench, limiters 25 of the rail travel 18 are installed.

The bench suggested herein works as follows.

When studying the adhesion of wheel 7 to the rail by means of the hydraulic jack 19, the required vertical load is applied through the spring suspension elements 9. Braking on rail 18 is is achieved by means of an electromagnetic brake. When current is applied to the coils 22, the latter are pressed against the side surfaces of the rail 18, generating a certain resistance force for its movement along the rollers 13 and 14, depending on the value of the supplied current.

Electric motor 2 spins flywheel 3 to a preset speed, torque converter 4 is filled with oil and transmits the torque through the reversible gearbox 5 to wheel 7. Under the impact of the adhesion force of the wheel 7 and the rail 18, the latter moves along the rollers 13 and 14 along the electromagnetic brake (if the adhesion force exceeds the resistance to movement created by the electromagnetic brake), and the sensors installed between the stops 23 of the coils 22 and the protrusions 24 of the bench frame continuously register the adhesion of the wheel with the rail. In this case, with the help of mechanisms 20 and 21, vertical and horizontal transverse dynamic loads with independently adjustable amplitude and frequency of disturbance are applied to the wheel 7, as well as signals from the sensors of adhesion force, vertical static load, wheel and rail speed are fed to amplifiers and further to the recording equipment. The length of the test process depends on the speed of the rail 18. When using the working length of the rail 18, oil is automatically drained from the torque converter 4 and the transmission of torque to the wheel 7 is stopped. The inertia of the moving parts is damped by the brakes until they come to a complete stop.

Prior to or during the testing, contaminants are applied to the rail that correspond to the operating conditions, and sand or other abrasive materials are also fed into the wheel-to-rail contact zone.

When testing the elements of axle spring suspension (axle drives, shock absorbers, etc.), the bench works in a similar manner. In addition to these parameters, signals from the sensors of the load and the travel of spring suspension elements are also recorded. By adjusting the distance between the rollers 13 and the point of contact of the wheel with the rail using the lift mechanism 16, one can change the vertical stiffness of the simulator of the railway track, and changing the distance between the rollers 15 and the point of contact of the wheel with the rail using the lift mechanism 17 will change the horizontal stiffness of the simulator of the railway track, thereby helping one conduct the studies with varying the rigidities.

On the bench described above, studies of the adhesion coefficient were carried out. The results of the dependence of the adhesion coefficient on various factors are set forth in [18].

Table 1

Technical characteristics of the test bench for studying the wheel-to-rail adhesion

Rail type and length, m	P50, P65, P75; 12.5
Wheel diameter, m	0.76 ... 1.25.
Vertical forces pressing the wheel to the rail, kN	60 ... 135.
Tractive force, k.N	0 ... 60.
Dynamic vertical forces, kN	0 ... 20.
Dynamic force frequency, Hz	0 ... 40.
Travel speed m/s in the mode: traction coasting	 0 ... 5. 0 ... 40.
Generated adhesion coefficients	0.17 ... 0.57.
Wheel drive	Electric inertial with hydromechanical transmission
Rail brake	Magneto-rail
Braking modes	Service and emergency
Measured and recorded parameters	Adhesion force, vertical force, lateral force, relative slip, travel speed, rotation speed
Force measurement method	Tension dynamometers
Speed and slip speed measurement methods	High-speed filming, video camera, magnetic disks, magnetic recording, magnetic field
Preliminary travel measurement method	Laser sensor

3.2. Measurement of frictional characteristics of a railway track

The existing test benches make it possible to study the process of adhesion of the driving wheel to the rail in laboratory conditions. However, the only difficulty that is difficult to reproduce in the laboratory is the actual contamination of the rail by the products and to the extent that exist on various sections of the railway track. Therefore, for such measurements in order to subsequently reproduce their results in laboratory facilities, as well as to refine the initial data of mathematical models, measuring devices are required that can be easily transferred from one section of the track to another. Such devices that measure the frictional properties of surfaces are called friction machines or tribometers.

The existing friction machines do not allow fully and sufficiently reliably measuring the friction characteristics of the wheel-to-rail contact pair, since they measure the friction coefficient in the mode of pure sliding friction (slip) of the contacting surfaces. However, in the wheel-to-rail system, in addition to this, the rolling mode with sliding is generated.

For this, a special, customized friction machine was designed to promote the study of frictional properties of the wheel-to-rail contact. It comprises two parts: (1) a friction machine (Fig. 7) that consists of a bogie, orienting and measuring units; and (2) a linear speed controller.

The bogie is a frame 1 and a system of levers and rollers 2, with which the frame is attached to the rail 21, with the possibility of linear movement along its axis. The bogie is designed to carry the orienting and the measuring units.

The orienting unit comprises guides 3, segments 4, levers 5 and a crossbar 6. It is designed to orient the working roller 7 along the normal line to the destination point of the rolling surface of the rail 21. The roller is oriented by the segments moving along the guides 3; the levers 5 turned relative to the segments, and the crossbar 6 moving along the guides of the levers 5. The orienting unit rigidly fixes the working roller in the required position.

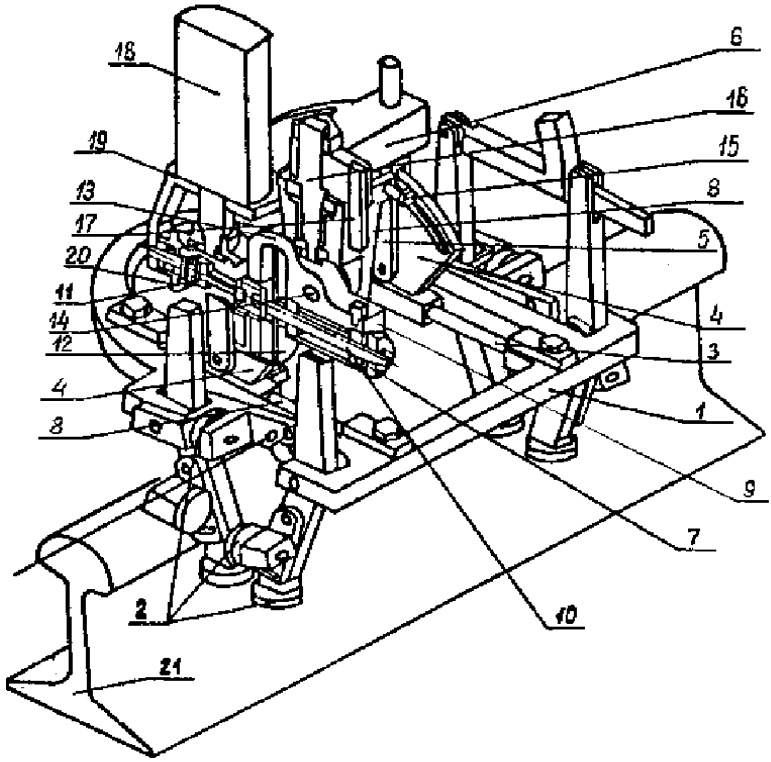

Fig. 7. Diagram of the moving part of the friction machine

The measuring unit is designed to transmit the vertical force and the torque to the working roller, as well as to measure the vertical force, angular speed of the working roller and the friction force of the roller on the rail. The measuring unit comprises the part 8 and the part 9. The part 8 is rigidly connected to the axis 14. The latter is coupled with part 9 through bearings (not shown in the figure). This kind of coupling provides a relative rotation of parts 8 and 9 in a plane perpendicular to the rail axis.

Levers (not shown in the figure) are rigidly mounted at the ends of the axis 14. Following the orientation and bringing the working roller into contact with destination point of the rolling surface of the rail with the help of bolts 15, which are screwed into the bracket of the body part 9, the body part 8 is rotated relative to part 9. Since the working roller is in contact and further rotation of part 8 is impossible, it is loaded with vertical force.

Tension sensors (vertical effort sensors) are pasted on the levers that are fixed at the ends of the axis 14. On the axis 16, which is rigidly fixed to the crossbar 6, a housing part 9 is inserted through the bearings, which allows the part 9, together with 8, to make angular rotations in the horizontal plane. The possibility of such a rotation is prevented by the lever 17. One end of the lever is rigidly fixed to the crossbar 6, and the other is connected to the part 8 so that the latter can be angularly rotated relative to the part 9 in a plane perpendicular to the rail axis. Lever 17 is equipped with tensor sensors that measure the friction force of the roller on the rail.

The torque from the motor 18, located on the platform 19, which, with the help of brackets rigidly connected to the crossbar 6 through the bevel gear 20, is transmitted to the propeller shaft 11, then to the axis 10 and the working roller 17. Speed sensors of the working roller 12, 13 are fixed on the axis 10.

The purpose of the bogie linear speed controller is clear from its name. The regulator consists of a winch 2 and a tensioning unit 3 (Fig. 7). The winch is equipped with a motor 4, worm gearbox 5, drive disc 6 and guide rollers 7. The drive disc and the tension roller 10 are tied by the cable 8. Roller 10 is mounted on a bearing and secured to lever 11. The cable 8 is tensioned by rotating the lever with the bolt 12. To measure the speed of rotation of the tension roller (linear speed of the bogie), it has a sensor.

The choice of a worm gearbox for the winch is mandated by two factors. Firstly, it largely allows you to open the power circuit: bogie - cable - drive disc - gearbox - motor. Secondly, the speed of rotation of the worm gear wheel is determined by the speed of rotation of the worm, i. e. there occurs a kinematic opening of the specified circuit.

The foregoing explains the operation of the linear speed controller of the bogie. The linear speed is set by the rotational speed of the motor 4 (worm) and does not depend on the tractive force developed by the working roller 7.

As indicated earlier, the vertical force sensors are represented by the levers mounted on the ends of the axis 14, and the lever 17 serves as the sensor of friction force of the working roller on the rail. Tensor sensors are pasted onto all levers, which are connected to the 8UNCH strain amplifier. The signals are recorded by the L-1221 precision board and transmitted to the computer.

The sensors were calibrated using a special device that was attached to the bogie frame. The working roller was replaced with a calibration roller and the end of the cable was attached to it. The cable was thrown over the block system and the weights were hung on the other end of the cable.

The level of specific pressures in the contact zone of the working roller with the studied surface can be regulated by changing either the load on the roller or the shape of its surface. The first method is ineffective, since a two-fold change in the pressure level requires an eight-fold change in the toe load. Therefore, the second method was chosen - changing the shape of the surface at the same vertical load.

A feature of the friction machine is a fairly wide range of changes in the angular $(0...70)s^{-1}$ and the linear (0...2) m/s speeds of the working roller. Such a wide range of speed variations makes it difficult to determine the sliding speed of the roller relative to the rail.

To simplify the problem, it was decided to determine the linear speed of the working roller by the rotation frequency of the tension roller, which led to the determination of the rotation frequencies of the rollers (working and tensioning) with an acceptable accuracy (not worse than 1%). This kind of accuracy cannot be achieved with the help of frequency or induction sensors, since they have some inertia and, moreover, do not work well at low speeds. Therefore, a sensor free of any such deficiencies has been developed.

The principle of operation of the sensor is based on measuring the time interval required to turn the rollers (working or tensioning) at a given angle [7].

The sensor (Fig. 8) comprises the body parts 3 and 4, interconnected through the bearing 5. Part 3 is rotary and part 4 is stationary. Part 3 is holding two optocouplers (I and II) that comprise infrared photo-(1) and light-emitting diodes (2). The luminous flux from the photo- to the LEDs is carried over by the light guides milled in part 3. Part 4 with its hump moves into the corresponding recess in part 3 and trips the light guides. The special slots on the hump of part 4 would periodically open the light guides. The step between the slots is greater than the angle of the optocouplers. A total of 45 slots are made, which allows 45 measurements to be taken in one revolution of the roller (working or tensioning).

When the slot is aligned with the first light guide in the direction of the travel, a signal appears on it. This signal is transmitted to a precision board and then to a computer.

The electrical circuit of the friction machine control panel allows setting the motors of the winch and the friction machine both independent and sequential excitation by switching the corresponding toggles. It is also possible to turn on the motors separately, thereby allowing one to explore the modes of slipping in place and skidding. Voltmeters and ammeters are placed on the dashboard to monitor the power consumption by the motor and the speed of the machine.

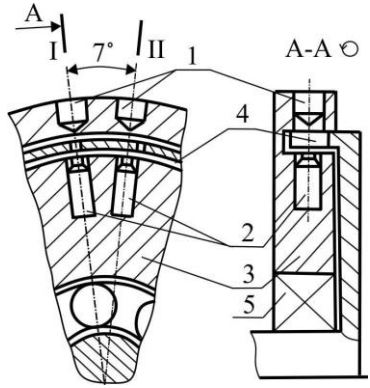

Fig. 8. Rotation speed sensor

The main parameters of the friction machine are set forth in the technical data sheet.

Technical characteristics of the friction machine

Bogie motor power, kW 1
Winch motor power, kW 1
Type of consumed current .....Direct
Excitation ..... Independent or consistent
Working roller diameter, mm ..... 20...40.
Load on the working roller, N ..... 200...2000.
Average specific pressure, MPa ..... 200...1400
Range of angular velocity variation, s^{-1} ..... 0...70.
Range of variation of the working
Roller traveling speed, m/s .....0..2

In addition to the frictional properties of the “wheel-rail” pair for various surface contamination, the influence of the material of the working roller on the sought dependencies was also studied. Work rollers are made of the following materials: St3, 40X and the tire steel in accordance with GOST 398-81. The experimentally measured hardness of roller materials was 180, 300, 250 HB, respectively.

It was mentioned earlier that the level of specific pressures in the contact zone of the working roller with the rail was regulated by changing the shape of the roller surface at the same vertical load (a load of 300 N was adopted on the basis of the experience of the experiments). All rollers were toroidal-shaped. Their diameter was 50 mm, and the radii of curvature were 700, 40, 12, 5 mm. With the accepted vertical load, this provided the following levels of average specific pressures: 300, 600, 900, 1200 MPa.

The shape of the surface of the rollers was carefully monitored and, if necessary, adjusted (rehabilitated) or the worn out roller was replaced.

Rollers made from the same material were made from one workpiece.

The average specific pressure level is as follows

$$\sigma_{cp}=P/F, \tag{3}$$

where P is the load on the roller;

F is the contact area of the roller with the rail. Attempts to determine F by the method of printing films or another method (copper plating, breaking strips) failed to provide the desired result, since no clear prints were obtained (due to the small contact area of the small diameter roller). In addition, methods such as copper plating or destructible films disrupt the frictional contact conditions.

Considering that the analytical solutions of the normal contact problem have been repeatedly tested experimentally, the contact area of the working roller with the rail was determined by the well-known formulas:

$$F = \pi ab;$$

$$a = 1{,}397 * n_a * \sqrt{\frac{P/E}{1/R_1 + 1/R_2 + 1/R_3 + 1/R_4}}\ ; \tag{4}$$

$$b = 1{,}397 * n_b * \sqrt{\frac{P/E}{1/R_1 + 1/R_2 + 1/R_3 + 1/R_4}}\ , \tag{5}$$

where - $n_a n_b$ - coefficients, the values of which are determined by the tables;

R_1, R_2, R_3, R_4 - radii of curvature of the contacting bodies;

E - Young's modulus.

Prior to each series of experiments, the sensors of the vertical load on the working roller and the friction force of the roller on the rail were calibrated.

The experiments were carried out in laboratory conditions at the air temperature of I6...25^{0}C and humidity of 60-80%.

The dependence of the coefficient of the friction of rest on the specific pressure in the contact area of the working roller and the rail was determined as follows:

- the winch motor was turned off, thereby fixing the position of the friction machine relative to the rail;
- a working roller made of the material under study and having the required curvature was fitted on axis 10 (see Fig. 7) ;
- voltage was applied to the motor 18 of the friction machine (a traction moment was applied to the roller), which gradually increased until the roller went into slipping;
- the computer recorded the load on the roller and the working roller tractive force;
- after the roller went into the slippingpin, the power of the bogie motor was turned off, the bogie would move someplace else, and the experiment would be repeated.

In total, 30-40 measurements were taken for each video. Then the working roller was replaced by a roller with a different curvature. The schedule of the roller breakdown into skidding is set forth in Fig. 9.

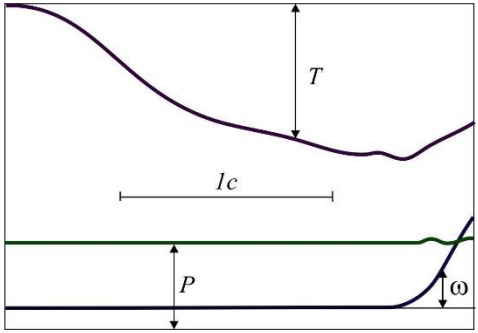

Fig. 9. Sample oscillograph of the working roller going into slipping in place

The application of the rolling roller method to study the sliding friction coefficient predetermined the experimental technique:

A working roller with a corresponding curvature was mounted on axis 10 (see Fig. 7), and a vertical force of 300 N was applied to it (the experiments were carried out only for rollers made of tire steel);

- using a winch, the friction machine was accelerated to specific linear speed 9 (total of four levels of the linear speed were taken: 0.1; 0.6; 1.1; 1.6 m/s).

After accelerating the machine, the voltage was supplied to the motor 18 (the torque was applied to the roller 7). The voltage would increase slowly until the roller would go into a slip. Then the car would be stopped and the bogie would

return to its original position. The experiment was repeated 7-10 times for each specific pressure level and each linear velocity.

In total, 150 experiments were made, from which up to 1,600 experimental points were taken for each of the frictional states covered by the study.

When studying the sliding friction coefficient on the rails coated with STP grease plus sand, after the very first pass of the working roller, a clear path was formed. Further work proved to be pointless, since the frictional conditions of contact changed, therefore this frictional state was excluded from consideration.

A sample graph of the process of rolling a working roller in traction mode is shown in Fig. 10. It records the vertical load on the roller *P*; the friction force *T* and the readings of the rotational speed sensors of the working and tension rollers (recorded in digital form).

The sliding speed is determined as follows:

$$V = R_p \omega_p - R_n \omega_n ,$$

where R_p, R_n - the radii of the working and the tension rollers respectively;

ω_p, ω_n - rotation speeds of the working and the tensioning rollers respectively.

One should separately address the methods for determining the temperature in the area of contact of the working roller with the rail.

Experimental determination of the temperature in the area of contact of the working roller with the rail faces great difficulties. A number of experimental methods are known. Unfortunately, since the contact is minute and short-lived, none of them can be used for the pair working roller - rail. Therefore, we used the well-tested computational technique of A.V. Chichinadze, from which the coefficient of distribution of heat flows was obtained.

$$\alpha = \frac{1}{1+\sqrt{\omega * R * N}}$$

Thus, by experimentally determining the friction force of the roller on the rail, the rotation speed and the forward speed of the roller, one will be able to find the temperature in the contact zone.

Test results of the friction machine obtained according to the described method, were processed using a special software is designed for a personal computer - and is written in C++.

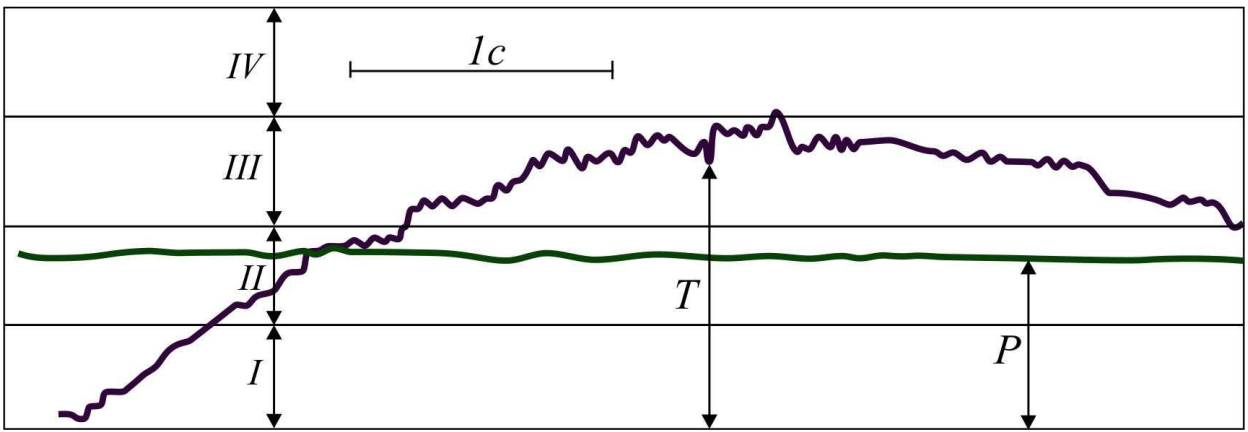

Fig. 10. Sample oscillograph of the travel of a working roller with sliding

The reference data are the results of calibration of the sensors and the results of experiments taken from the L1221 precision board.

To date, such analog-to-digital converters are widely used and are produced on an industrial basis. For example, the converters made by Hottinger Baldwin Messtechnik, Siemens, Schenk (Germany) [32], Bur-Brown [68].

This software approximates the calibration results, recalculates the readings taken from the precision board and performs statistical and regressive analysis using the least squares method.

Fig. 11 shows the dependence of the coefficient of friction on the specific pressure in contact at various frictional states of the rail surface and on the materials of the working rollers. These results are well described by the regression equation

$$f_0 = a_0 + a_1 * \sigma + a_2 * \sigma^2, \quad (6)$$

where f_0 – the coefficient of friction at rest;

a_0, a_1, a_2 – the correlation coefficients.

The values of the correlation coefficients are summarized in Table 2.

Table 2

Correlation coefficients of equation (6)

Frictional state of the rail	Roller steel grade	α_0	α_1	α_2
Covered with STP	tire steel	0.799990e-1.	0.2927230e-9.	-0.17525e-12
Covered with STP	Steel St3	0.899966e-1.	0.1026104e-8.	-0.61434e-12
	Steel 40X	0.700002e-1.	-0.487871e-10	0.292124e-13
STP + sand	tire steel	0.6420859e	-0.4189717e-3.	0.2238878e-6.
	Steel St3	0.5865017e	-0.3849275e-3.	0.1922944e-6.
	Steel 40X	0.5808506e	-0.2308477e-3.	0.6821200e-7.
Clean dry	tire steel	0.4671469	-0.3884749e-3.	0.2290456-
	Steel St3	0.4230729	-0.2928186e-3.	0.1513375e-6.
	Steel 40X	0.4663596	-0.2274798e-3.	0.5754208e-6.
Coated with diesel fuel	tire steel	0.2355543	-0.1813825e-3.	0.9493846e-7.
	Steel St3	0.2361088	-0.2044323e-3.	0.1065440e-6.
	Steel 40X	0.2799486	-0.2703010e-3.	0.1119114e-6.
Covered with water	tire steel	0.2522794	-0.9728668e-4.	0.5643096e-7.
	Steel St3	0.2915664	-0.1901969e-3.	0.9808301e-7.
	Steel 40X	0.3797418	-0.2790791e-3.	0.9226375e-7.

Even in the early stages of research [29], it was noticed that the physical coefficient of adhesion is influenced by a number of factors. Most of them can be considered the same for all wheelsets of a locomotive. Differences, as practice

shows, can only take place in connection with the so-called effect of rail cleaning by the front wheel. To obtain quantitative regularities and to determine the conditions for manifestation of this effect, the friction machine was redesigned. An additional roller was attached in front of roller 7, which did not rotate. The cleaning process was simulated by its sliding on the rail.

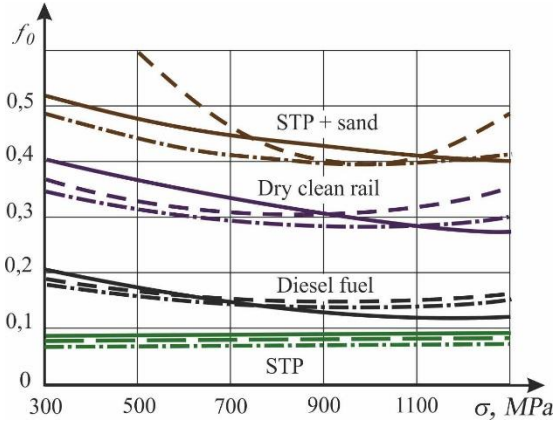

Fig. 11. Dependence of the coefficient of friction at rest f_0 on the contact pressure σ in various frictional states of the rail and on the material of the working roller:
——— Tire steel; ———— 40X; — · — · — · St3

The distribution functions of the friction coefficient are subject to the normal distribution law and have for each rail state:

- clean, dry

$$f = 34e^{-6128(f_0-0,56)^2}$$

- drenched in water

$$f = 14,5e^{-1753(f_0-0,34)^2}$$

- oily

$$f = 15,6e^{-903(f_0-0,157)^2}$$

For a roller running on a clean, dry rail, the coefficient of friction is nearly equal to that of a roller that is not equipped with a scraping roller. At the same time, its value does not change from the value of the generated tractive effort.

Therefore, it would be safe to assume that all wheelsets of a locomotive moving on clean dry rails have approximately the same physical coefficient of adhesion. For a rail drenched in water, it is characteristic that the contacting conditions before each subsequent wheelset of the locomotive will change. Moreover, this change depends on the magnitude of the tractive effort generated by the frontal wheelsets. The same phenomena are observed for the oiled rail.

This can be explained by the improvement in the frictional state of the "wheel-to-rail" contact due to its mechanical cleaning and removal of contaminants, as well as due to the evaporation of water or a change in the state of the oil film.

Analysis of the results of an experimental study of the dependence of the sliding friction coefficient on the specific pressure, sliding speed and temperature in the contact zone made it possible to exclude the sliding velocity from consideration, and the problem was reduced to determining the dependence

$$f = f(\sigma, \Theta).$$

The experimental results are set forth in Fig. 12. Experimental points are best described by the equation

$$f = \alpha_0 \theta^{a_1} e^{a_2 \theta^k} \left[(\sigma - 300)/1000\right]^{a_3}, \qquad (7)$$

where Θ, σ - respectively the temperature and the specific pressure in the contact zone;

a_0, a_1, a_2, a_3 – the correlation coefficients;

K – the coefficient that was selected individually for each frictional state.

The values of the correlation coefficients and the coefficient k for various frictional contacting conditions are summarized in Table 3. When comparing the results of the study of the coefficient of static friction (Fig. 11) and the coefficient of sliding friction (Fig. 12), one can't help noticing the fact that for all frictional states the maximum coefficient of sliding friction during the sliding travel turned out to be higher than the coefficient of static friction. This is especially pronounced on rails covered with diesel fuel. To explain this fact, let us turn to [12], where typical results of the effect of temperature on the friction of solids lubricated with palmitic acid with borderline lubrication are described. When the temperature rises to 69°C, the first rupture of the lubricant film occurs and the friction coefficient increases sharply. At 120°C, the second rupture of the film is observed and the coefficient of friction becomes the same as for non-lubricated surfaces. A similar result was obtained in [50; 64], where an abrupt increase in the sliding friction coefficient was observed with an increase in temperature in the contact zone due to the relative friction. When rolling with sliding, this relationship takes a different form.

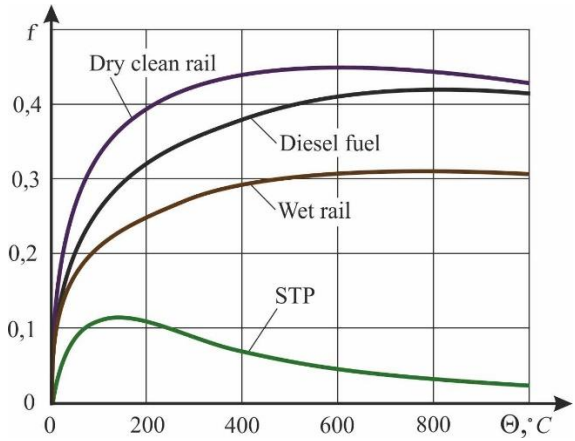

Fig. 12. Dependence of the coefficient of sliding friction during the rolling with sliding on the temperature Θ in the contact zone (σ =300 mPa) at various frictional states of the rail

Table 3

Correlation coefficients of equation (7)

Frictional state of the rail	K	α_0	α_1	α_2	α_3
STP	0.6	0.40911e-2.	0.10341e+1.	-0.29166- I	0.89379
Clean dry	0.6	0.58985e-1.	0.43134e+0.	-0.15889e-1.	0.86335
Coated with diesel fuel	1.75	0.61733e-1.	0.30199e+0.	-0.14820e-5.	0.82739
Covered with water	1.75	0.60544e-1.	0.27087e+0.	-0.14738e-5.	0.83679

Fig. 13 shows a selection of experimental points plotted on the coordinate plane of temperature Θ coefficient of friction f for all levels of linear speed of the friction machine (the rail is covered with diesel fuel, the average specific pressure in the contact of the working roller with the rail is 300 MPa).

A sharply defined crest is seen in Fig. 13 in the temperature range of 20...30°C. Its presence can be explained by a change in the physicochemical state of the rail surface due to the heat release in the contact. In this case, first of all, the bearing capacity of the surface contamination film is disrupted. Any further increase in the temperature (sliding speed) leads to a result similar to that described earlier: the coefficient of friction becomes the same as for non-lubricated surfaces.

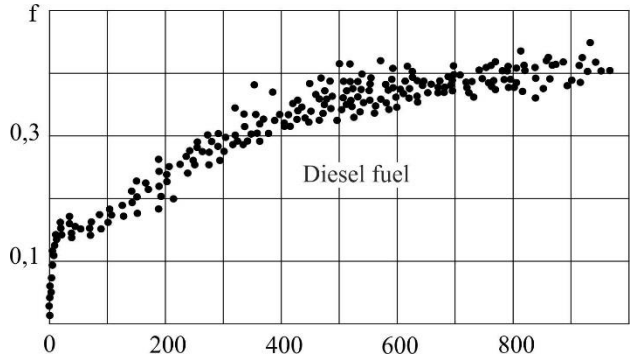

Fig. 13. Experimental dependence of the sliding friction coefficient on temperature in the contact zone (σ = 300 MPa)

As the working roller goes into slipping, the friction force can rise, fall, or remain unchanged. Since the purpose of this study was not to study the development and termination of the slipping, we will offer just a few comments.

During the experiments, the working roller would stop slipping all of its own occasionally. What makes these experiments special is that no action was taken by the operator of the friction machine after the start of the slipping. The friction force would decrease, and then it would grow until the slipping has stopped. After the slipping was over, the frictional force would exceed its own initial value by 2 times or more. The process of self-terminating slipping is described in detail by G.V. Samme [67].

With an increase in the supply voltage of the motor of the friction machine, the slipping would not stop for a sufficiently long time (out of fear of damaging the friction machine, the slipping time was limited to 15...20 s). In addition, on the rails coated with the STP grease, getting the slipping to self-terminate proved to be generally impossible.

Thus, recognizing the presence of the second maximum of the adhesion characteristic, one should note the complexity and ambiguity of the slipping process and the uncertainty about the guaranteed use of the phenomenon of the increase in the adhesion coefficient with a large relative slip (spin).

Based on the analysis of the obtained results, one may conclude as follows:

- the presence of a minimum dependence of the coefficient of static friction on the specific pressure ranging from 800 to 1000 MPa was confirmed;
- the material of the contacting bodies has a quantitative and qualitative effect on the dependence.

Under the very poor contacting conditions, the coefficient **of** friction at rest appears to be independent of both the materials of the contacting bodies and the specific pressure in the contact.

When rolling with sliding and at a certain level of the sliding, maximum obtained coefficients f appear to be higher that coefficients f_{ad}, measured in the same contacting conditions for each friction state on the surface.

3.3. Simulation of the ties between the wheel and the rail at point-to-point contact

During the movement of the vehicle along the railway track, especially in curved sections, the wheel flange remains in contact with the rail head for a considerable time. This is when occurs the most intense dynamic interaction of the vehicle and the track in the transverse direction. Therefore, modeling of forces at the two-point contact of the wheel with the rail is of great importance when considering the locomotive motion.

A significant number of works deal with this issue. Most of them proceed on the assumption that the connection between the wheel and the rail is inseparable and sustainable, and the contact is assumed to be a single-point. After choosing the clearance in the track D, a rigid connection is applied to the wheel-on-rail motion [4]. Further motion of wheel and the rail occurs in concert as follows:

$$y_p = y_w - D;$$

$$Y_p = S * y_p * \delta(y-D);$$

$$S_y = F_y(1-\sigma(y - d)) + Yp, \quad (8)$$

where - Y_p – the lateral reaction of the rail;

δ - the Heaviside step function;

y – the lateral motion of the wheel relative to the rail;

y_p – the lateral motion of the rail;

y_w – the lateral motion of the wheel;

D – the lateral motion of the wheel; when exceeded, the wheel would roll onto the rail;

S_y – the lateral horizontal component of the vertical load;

F_y - the transverse component of the adhesion force.

S – the transverse stiffness of the rail.

In another case [5], when the wheel flange is in contact with the rail head, a change in the tangent of the tilt at the contact point is simulated, wherein lateral horizontal forces would increase sharply:

$$\begin{aligned} &\mu = 0{,}05 \text{ at } -D < y < D, \\ &S_y F_y (1 - s(y - D)) P\mu, \\ &\mu_1 \text{ at } |y| > D, \\ &S_y = F_y (1 - s(y - D)) + P\mu_1. \end{aligned} \tag{9}$$

where P - the vertical load from the wheel on the rail;

tg(g)- the tangent angle of the tilt against the contacting surfaces at the point of contact;

μ - the wheel slope;

μ_1 – the coefficient (0.187106 [m-2], [5]).

With these models, point-to-point contact is not considered. Meanwhile, wheels with new rolling profiles are being in contact for a considerable time with the rail head with the ridge and the rolling surface simultaneously. In this case, the results of calculations based on the above models do not reflect the real processes. In addition, when assessing the dynamic qualities of vehicles, one should make provisions for the possibility of the wheel flange crawling onto the rail head to assess the safety of motion.

Let us study the action of forces between the wheel and the rail at the two-point contact (Fig. 14)

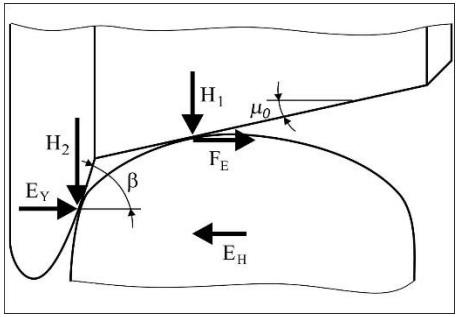

Fig. 14. Diagram of the two-point contact of the wheel with the rail.

The load from the wheel to the rail is distributed over the tread track and the ridge:

$$H_1 + H_2 = H. \tag{10}$$

As it follows from Fig. 14:

$$H_2 = (Yp - Fy)(f\sigma(y) + 2ctg(\beta)). \tag{11}$$

Once the entire load from the wheel to the rail is transmitted only through the ridge, i.e. when $H_2=H$, the wheel flange crawls onto the rail head.

Then

$$S_x = F_x - f / sin(\beta)Y_p$$

$$S_y = F_y - Hl\mu - H_2 * tg(\beta)$$

$$S_z = H - H_2$$

$$F = f(\varepsilon, H_1)$$

$$F_x = F\varepsilon_x / \varepsilon$$

$$F_y = F\varepsilon_y / \varepsilon$$

whereε - the slide of the wheel relative to the rail.

S_x - the longitudinal force in contact of the wheel with the rail;

S_z - the vertical contact force;

x - the longitudinal component of the adhesion force;

f – the coefficient of friction of the wheel flange on the rail head;

β - the ridge tilt angle.

In this case, unlike the previous one, the wheel-to-rail adhesion force is determined depending on the vertical load at the point of contact of the tire with the rail. The force of the transverse interaction of the wheel with the rail is determined, in addition to the transverse component of the adhesion force, by the ratio of the values of the vertical forces in the contact points of the tire with the rail and the flange with the rail head.

To evaluate the performance of each model, a series of calculations was carried out using the motion of a single wheel pair in a railway track as an example [1]. Motion in curved track sections is considered in the same manner as in [3].

According to the findings of the analysis, the method of modeling the two-point interaction of the wheel with the rail affects the values of dynamic forces obtained through calculations.

When moving on a straight section of the track in a coasting mode at 25 m/s, for (8*)* Y_P was 21.28 kN, for (9) 17.26 kN, (10) - 17 kN, and for (11) - 15.7 kN.

3.4. Modeling the adhesion force when solving the problems of the wheel motion on the rail

All the works mentioned hereinabove handled the contact problems by using the classical approach originated by G. Hertz that implies the use of singular integral equations. However, the theory of G. Hertz is not always suitable for handling

of the contact problems of wheel-to-rail interaction [5, 85]. At the same time, in connection with the emergence of electronic computers and their intensive development, numerical algorithms have been developed for this purpose, for example, using the finite element method [2, 5, 6], the method of nonlinear boundary equations [11], etc.

[24, 27, 30, 44, 43, 45] solved the problem of determining the adhesion coefficient of a locomotive wheel to the rail surface on the basis of frictional and temperature processes in the contact area.

The adhesion model is based on the sequential solution of two problems - normal and tangential. The normal problem was solved through representation of the contacting bodies in the form of elastic half-spaces using the numerical methods [45]. Solving the normal problem will help determine the coordinates of the points of the initial contact of the wheels(wheelset) with the rails, the shape and the size of the contact patch (area E) of the wheel with the rail, and the distribution of normal tensions along it $\sigma(i,j)$ (Fig. 15). These results represent the initial data for solving the tangential problem.

The purpose of solving the tangential contact problem was to determine the adhesion force of the locomotive (wheelset) wheel with the rail (railway track). The rolling locomotive wheel is pressed against the rail by the effort r_z and it moves at v. Under the impact of effort r_z, contact zone E is formed due to the elasticity of the materials of the wheel and the rail. The shape and the size of the zone E , the distribution of normal stresses over it, as well as the pressing effort r_z are determined in the course of solving the normal contact problem. In addition, the preset values are the law of friction (the dependence of the coefficient of friction on temperature and pressure in the contact $f(\sigma, \Theta)$, which was obtained experimentally (see Fig. 6)), the elastic and thermophysical properties of the contacting bodies. Solving a dynamic problem will help finding the relative slip vector $\vec{v}$ -.

To solve the problem, one should use a rectangular mesh of MxN with sides Δi, Δj plotted on the common plane for the wheel and the rail.

The rolling and the sliding process was considered stationary. It was also assumed that the speed of the locomotive is much less than the elastic perturbations in the contacting bodies (a quasi-static problem). With this in mind, the task is formulated as follows: for the preset distribution functions of normal pressures $\sigma(i, j)$, slides $\vec{v}\ (i, j)$, the dependence of the sliding friction coefficient in rolling with sliding $f(\sigma, \Theta)$ on temperature Θ and contact pressure σ in E, find the vector function of tangential stresses $\vec{\tau}\ (i, j)$ by

$$\vec{\tau} = \sigma(i, j) f(\sigma\Theta)\vec{v}\,|\vec{v}\,|, \tag{12}$$

where the function $f(\sigma, \Theta)$ is determined experimentally.

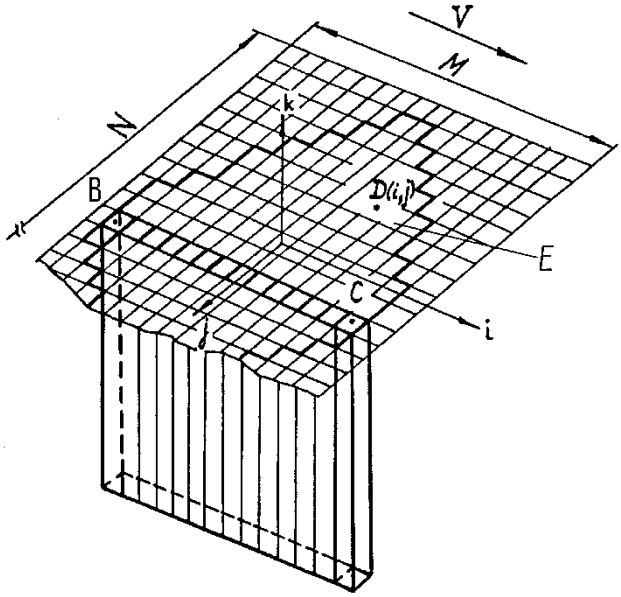

Fig. 15. Design scheme of the wheel-to-rail contact condition

Then the adhesion force of the wheel of the locomotive with the rail is^

$$\vec{F}_{ad} = \int_E \vec{\tau} dE .$$

To calculate $\vec{\tau}$,one needs to determine the temperature field by the contact spot. This field is found in the course of solution. To determine the latter, let us consider point *D(i, j)* in the contact zone and pertaining to the rail (Fig. 11). Within E , there is an active distributed heat source with an intensity of

$$g(\Theta) = \alpha \sigma(i, j) f(\sigma, \Theta) |\vec{v}(i, j)| , \qquad (13)$$

where α - the coefficient of distribution of heat flows (taken as 0.5). The intensity of the source varies and depends on the specific pressure, temperature in the contact zone, and the local value of the slide vector.

Temperature in point *D* at $t=l/v$,

where l - the distance from the leading edge to point *D* along the axis $O_A i$;

v - the speed of the locomotive that can be determined by solving the non-stationary problem of heat conduction, which, in the case of the independence of the thermophysical properties of the materials of the contacting bodies from temperature, appears to be as follows:

$$\beta\left(\frac{\partial^2 T}{\partial i^2}+\frac{\partial^2 T}{\partial j^2}+\frac{\partial^2 T}{\partial k^2}\right)\pm q = c\theta\frac{\partial^2 T}{\partial t}, \qquad (14)$$

where β - the coefficient of thermal conductivity;

c_ρ - the volumetric heat capacity;

q - the distribution of the heat source;

T - the temperature;

t - the time.

No analytical solution to problem (13), (14) has been obtained and therefore it was carried out by a numerical method.

Additional assumptions have been made:

1. The points of the wheel and the rail, once in the contact zone, move parallel to the axis O_Ai. The admissibility of such an assumption is due to the short duration of a single contact (only 10^{-3}. ..10^{-5} s). With this in mind, movement in the direction of the O_Aj axis can be neglected.
2. The heat generated by the relative sliding of the contacting surfaces spreads only along the normal to the latter. The assumption is correct for the Peclet number

$$Pe = vl/a > 20, \qquad (15)$$

where v - the speed of the locomotive;

l - the contact length;

a - thermal diffusivity of the wheel and the rail materials.

For the actual dimensions of the contact pads and the locomotive speeds, condition (15) is fulfilled.

What follows from this assumption is the ability to model the interacting bodies by a set of rods with thermally insulated side walls, and problem (14) for each rod forming a wheel and a rail will be simplified:

$$\beta\frac{\partial^2 T}{\partial i^2}\pm q = c\rho\frac{\partial T}{\partial t}. \qquad (16)$$

Functions $\sigma(i, j)$, $\vec{v}\ (i, j)$, and $\vec{\tau}\ (i, j)$ are considered piecewise constant, and in a certain cell with center m, n

$$\sigma(i,j)=\sigma(i_m,j_n);\vec{\tau}(i,j)=\vec{\tau}(i_m,j_n);\vec{v}(i,j)=\vec{v}(i_m,j_n).$$

The contact spot is considered as the sum of N stripes parallel to the O_Ai axis (Fig. 15). First, the adhesion force was determined for each of the strips, and then - for the entire contact patch. This representation of the contact patch is associated with the above assumptions.

To determine the temperatures, we used the analytical dependence of calculating the temperature in a rod with heat-insulated walls under the action of a flat heat source over a certain period of time [20, 41].

$$T = \frac{2q\sqrt{t}}{\sqrt{\lambda c\rho}}\left[\frac{1}{\sqrt{\pi}}e^{\left(k^2/4at\right)} - \frac{-k}{2\sqrt{at}}Erfc\left(\frac{-k}{2at}\right)\right] \qquad (17)$$

Since only the temperature on the surface of the contacting bodies is required, then at k=0 the expression would suffice

$$T = \frac{2q\sqrt{t}}{\sqrt{\lambda c\rho}} \qquad (18)$$

The package of bars numbered 1 through N is considered again with cross section $\Delta i x \Delta j$, (Fig. 15). The upper ends of the rods in the contact plane form a BC strip with number n $(1 \le n \le N)$ that is parallel to O_Ai. Each rod in the strip n is numbered m $(1 \le m \le M)$.

The assumption is that upon entering the contact zone in the direction of the motion, at point C (Fig. 15) and for a period of time $t = \Delta i/v$, where Δi - the step of the surface grid along the axis O_Ai, it is subject to heat source q_1 the power of which is determined in accordance with formula (16).

The initial temperature distribution along the length of the rod was assumed to be known and equal to zero, and the power during time $t = \Delta i/v$ of the heat source constant.

Since the power of the source depends on the temperature in the contact, problem (16) was solved with successive refinement of the value $q(\Theta)$ by way of the simple iteration method. At the same time, the value $\bar{\tau}\ (i_m, j_n)$ acting on the end of the m-th bar (in the contact plane) was determined. After the acceptable accuracy of determination $q(\Theta)$ was attained, the research would move on to the next rod. On the second rod, over the same period of time t, the heat source q_2 would be active, whereas source q_1 would cease. Therefore, the temperature change in the rod from q_2 was calculated and the temperature change that occurred after the end of the action of q_1 after the time t was added, which was determined as the difference between the temperature caused by the action of the positive source q_1 during the time $2t$ (two rods passed) and the temperature from the negative source q_1 of the same intensity over the time t.

The value of q_2 would be refined once again. On the third rod, the temperature change due to the action of q_3 was determined and the temperature changes in the rod were added, which occurred after the end of the action of q_1 and q_2, determined as the difference between the temperatures caused by the action of the positive q_1 over the time $3t$, and the negative q_1 over the time $2t$, and between the temperatures caused by the action of the positive q_2 over the time $2t$ and the negative q_2 over the time t.

The value of q_3 was refined. This was repeated M times, after which the research would move on to the consideration of the next contact strip. For the first rod in the direction of the motion, zero initial conditions were assumed again.

Since refining the power of the heat source q went along with calculation of the value $\vec{\tau}\,(i_m, j_n)$, the adhesion force was determined by the formula:

$$F_{ad} = \sum_{m=1}^{M}\sum_{n=1}^{N}\sqrt{\tau_i^{\,2}}\,(i_m, j_n)\Delta i\Delta j \qquad (19)$$

The order of summation in formula (19) is based on the above assumptions.

This solution properly describes the one-point contact of the wheel with the rail. However, for a considerable time in the process of movement, the wheel and the rail can be in the so-called two-point contact, especially when passing curved sections of the track. In this case, the rolling surface of the wheel tire and the rolling surface of the rail and the flange simultaneously interact with the lateral surface of the rail. At the same time, very intensive processes take place, directly affecting both the traction and the dynamic characteristics of the vehicle.

In this case, the researcher faces two pressing problems: determine the distribution of forces over the two points of contact and, on this basis, calculate their shape and size and the distribution of pressures.

The previous section shows the mechanism for determining the dynamic forces that act in contact. They can be determined in the process of solving the dynamic problem of the railway vehicle motion. This way, we find the solution to the first problem.

Based on these results, one can find a solution to the normal contact problem, i.e. determine the shape and the size of the contact spots and the distribution of normal contact pressures over them. However, an additional problem arose here related to identification of mutual influence of the contact patch on the wheel flange and on the rolling surface of the tire.

According to calculations, any significant elastic deformations of the wheel surface under loads of the order of 100 kN practically attenuate at a distance of 3-4 mm from the contact spot boundary (less than 1%), which is an order of magnitude smaller than the spot size. On the one hand, this is a consequence of the principle of the theory of elasticity about the locality of loads, while on the other hand, a consequence of the fact that along the boundaries of the contact spot the values

of normal contact pressures are minimal, getting closer to zero and attenuation. Similar processes take place on the rail surface.

Thus, given that the distance between two contact spots significantly exceeds this value (manifold), on the basis of the developed model of adhesion, we can calculate the adhesion force for the two-point contact of the wheel with the rail, addressing each contact separately and independently of each other.

Fig. 16, 17, 18 represent the dependencies $\psi(\varepsilon_{ck})$ for various speeds of the wheel on the rail, the state of the contacting surfaces and vertical wheel-to-rail loads, obtained by solving this model of adhesion, the results of which are well in concert with the experimental data obtained by a number of authors [95, 92, 74, 75, 80, 66, 63, 55]. However, there is still no sufficiently substantiated experimental confirmation to this theory. Therefore, before using it, one would have to carry out a large amount of experimental work. The advent of computers over the last decade has also stimulated the development of nonlinear programming methods and variational methods for solving the contact problems [46, 6, 5].

Meanwhile, the obtained results make it possible to use this model in the equations of locomotive motion.

In this work, a numerical experiment was carried out, resulting in attainment of the regression equations that describe the process of interaction of the wheel and the rail under various contact conditions:

$$\vec{F}_{ad} = P\frac{\vec{S}}{|\vec{S}|}/\left(A_1/\exp(\varepsilon B) + A_2\ln(\varepsilon B) + A_3/(\varepsilon B) + A_4(\varepsilon B) + A_5\right)\times \times T_2T_4/T_7T_8 \quad (20)$$

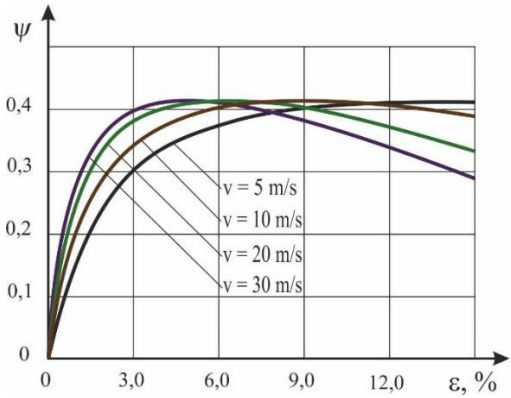

Fig. 16. The dependence of the adhesion coefficient on the slip built according to [24, 27, 30, 42, 43] for various speeds

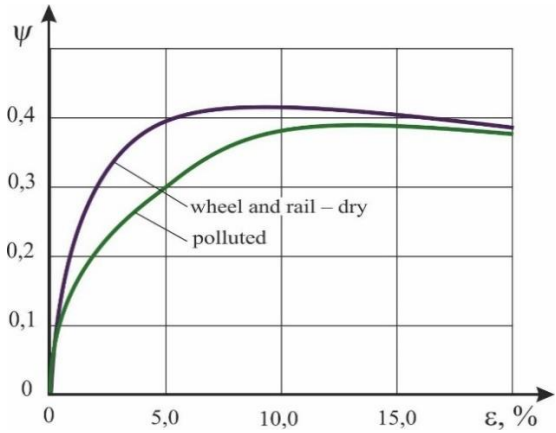

Fig. 17. Dependence of the coefficient of adhesion on the slip built according to [24, 27, 30, 42] for various frictional states in the wheel-to-rail contact

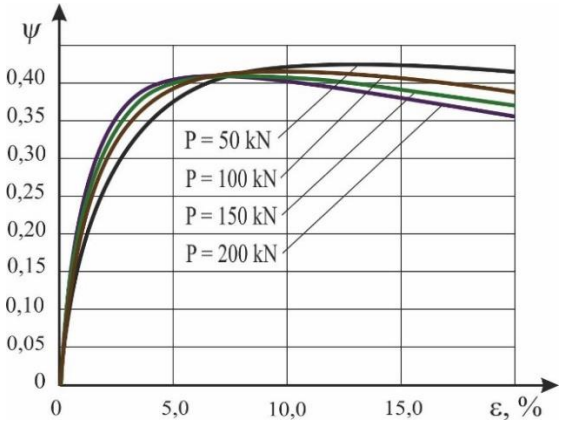

Fig. 18. The dependence of the coefficient of adhesion on the slip built according to [24, 27, 30, 42] for various vertical loads from the wheel to the rail

where A_1, A_2, A_3, A_4, A_5 - the coefficients of the equation;

$\vec{S}$ - slide vector;

ε - relative slip, [%];

$B=T_1T_3T_5T_6$; T_1, T_2 - coefficients taking into account the frictional state of contact surfaces, T_3, T_4 - vertical load, T_5 - speed of movement, T_6, T_7 - lateral movement of the wheel relative to the rail, T_8 - angle of attack φ.

Coefficients of equation (20) for various combinations of contacting bodies are set forth in Table 4.

Table 4

Regression equation coefficients for determining the wheel-to-rail adhesion force for various combinations of contacting bodies

	a)	b)	c)
A_1	0.754629766265	0	0
A_2	-0.22379766858	-0.1419381	-0.193
A_3	2.2154859175	0.026201	0.0379415
A_4	0.0476785	4.3642	3.31448
A_5	2.218	2.0729	2.115
T_1	0.009+2.38μ	0.026+2.38μ	0.026+2.38μ
T_2	0.4164/μ	μ/0.40907	μ/0.406
T_3	1/(9.18$P^{0.479}$ - 0.011) P [kN]	0.635 + 0.00368P	12.4/(23.89371-0.16353P+0.000476P^2)
T_4	1.026-0,000194P-0.0000012P^2-0.0000000053P^3, P[kN]	0.9713+0.0003454P-0.0000005674P^2	0.429348-0.0000696802P
T_5	1/(3.498$v^{-0.536}$--0.018), v [m/s]	(0.10108v-0.108)$^{0.5}$	12.25/exp(-.523ln(v) +3.725)
T_6	0	1.0002+0.1026y+0.002419y^2 -0,000728y^3, y [m]	12.25/(0.0000050377/exp(y)+ +0.000352571y^2 ++ 0.083), y[mm]
T_7	0	0.99976+0.0059684y-0.00006288y^2 0.0000577856y^3, y[m]	1/(0.00000747/exp(y) 0.00063638y +2.37), y [mm]
T_8	0	1-0.0056|φ|(0.1057 +0.087y+0.01156y^2)) φ [rad]	0

Here μ - the value of the maximum coefficient of adhesion, previously determined for specific frictional conditions according to the above model of adhesion, i.e. maximum on the adhesion characteristic.

Table 4 uses the following designations: a) the case of contact of new locomotive wheel profiles (GOST 11018-87) and R65 rail (GOST 8161-75) (Fig. 19, 20); b) a worn-out wheel profile, the so-called "stable profile" (Fig. 21), built on

the basis of the analysis of the wear of locomotive wheels in [77], and a new R65 rail (GOST 8161-75); c) a worn-out wheel and a worn-out rail [77] (Fig. 22).

Whereas μ characterizes the frictional state of the contacting surfaces of the wheels and the rails, we will use the value of the maximum adhesion coefficient in further calculations to determine the frictional conditions of adhesion.

The mathematical model of adhesion developed in this section and the formulas obtained from it (20) are used to solve the traction and dynamic problems when modeling the vehicle motion on a railway track.

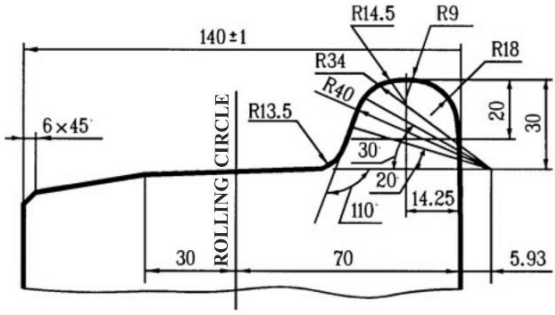

Fig. 19. Wheel profile according to GOST 11018-77

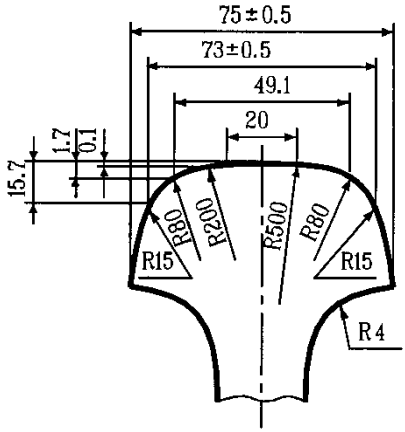

Fig. 20. R65 rail profile in accordance with GOST 8161-75

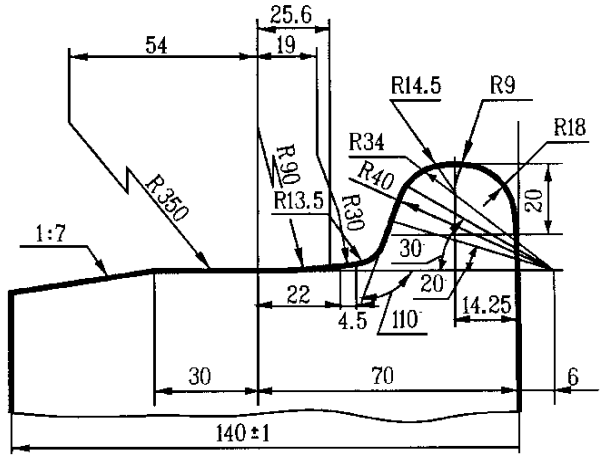

Fig. 21. Wheel profile according to [78]

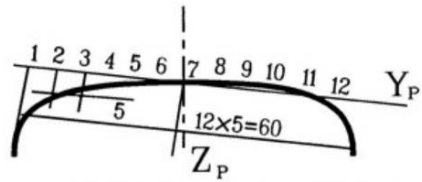

No. CONV. SECTION		1	2	3	4	5	6	7
COORDI-NATES	Y	-29	-27.5	-25	-20	-15	-10	-5
	Z	16	11	6.5	3.5	2.6	1.3	0.8
No. CONV. SECTION		8	9	10	11	12	13	
COORDI-NATES	Y	0	5	10	15	20	25	
	Z	0	-0.34	-0.56	-0.7	-0.74	-0.65	

Fig. 22. Rail profile according to [78]

3.5. Determination of the change in the radius of the wheel and the tangent of the angle of arrival at the point of contact with the rail

In mathematical models of the vehicle movement, the shape of the profiles is most often taken into account by two dependencies: $\Delta R(y)$ and $tg\gamma(y)$ - changes in the radius R of the rolling circle of the wheel and the tangent of the angle of arrival γ to the surface of the wheel and the rail at the point of their contact from the transverse travel of the wheel pair relative to the railway track y. These dependencies can be obtained both experimentally [81] and analytically [14, 33, 78, 94, etc.].

However, most works on the dynamics of the railway vehicles determine $\Delta R(y)$ and $tg\gamma(y)$ analytically, and most frequently [54, 13, 1] use the following expressions:

$$\Delta r(y_{ijn}) = (-1)^n \lambda y_{ijn}, tg\gamma(y) = \lambda, \qquad (21)$$

where λ- conicity (for new wheels in accordance with GOST 11018-87, the conicity is 1:20) or effective conicity [54, 13], which is

$$\lambda_{E^{TM}} = \lambda / (1 - r_p / r_\delta),$$

where r_p and r_δ - the radii of the profile of the rail and the tire, respectively.

The formulas (21) are approximate, since λ is assumed to be constant, which takes place only in the case of contact of unworn wheels with a conical profile with an unworn rail.

In [33, 78, 96, 94, etc.], the indicated dependencies were obtained on condition of the equality of the tangents of the angles of arrival to the surface of the wheel and the rail at the point of contact. The disadvantage of this approach is that one needs an analytical solution to the problem for all the studied combinations of the wheel and the rail surfaces. And this is not always possible with certain combinations of functions that describe the profiles. For example, worn-out profiles of wheels and rails cannot always be described by an analytical function with sufficient accuracy. That is why a tabular (dot) description method is used more frequently. In this case, the solution by the analytical method is impossible.

Another way to define $\Delta R(y)$ and $tg\gamma(y)$ was developed in [10]. The rolling profiles of the wheel and the rail are divided into sections, each described by the segment of circle equations. An analytical expression is then obtained for each sector, describing the clearance between the surfaces of the wheel and the rail. The point at which the clearance is minimal is the point of contact. Similar to the previous case, this approach provides a solution to a limited range of problems.

[31] describes the ways to identify the change in the radius of the rolling circle of a wheel, taking into account the lateral rolling and wobbling of the wheelset.

The point of contact of the wheel with the rail is found on condition of the minimum distance between their surfaces, taking into account the angle of lateral rolling of the wheelset. However, to obtain the desired dependencies, analytical descriptions of the contacting surfaces are used, thereby limiting the range of tasks in the same way as in the two cases hereinabove. Therefore, in [31], the values of dependence $\Delta R(y)$ are obtained only for a typical rail car wheel and P65 rail. Unfortunately, no results are presented in [31].

These disadvantages can be avoided by using the method described in [23] for determining the points of initial contact of the wheels and the rails at their arbitrary location, which was developed to solve the normal contact problem.

On its basis, this work develops a method for determining the dependencies $\Delta R(y)$ and $tg\gamma(y)$. The method appears to be as follows.

Let us consider a wheelset that is rolling along a railway track. We would introduce two left-hand orthogonal coordinate systems. System O_kXYZ is linked to the center of gravity of the wheelset, and the system $O_\rho\zeta\eta\xi$ - to the railway track, as shown in Fig. 23. The surface of the wheels is described in the coordinate system $O_{to}XYZ$ by the following equations:

$$Z_l = Z_l(X,Y) \text{ - for the left wheel;}$$

$$Z_r = Z_r(X,Y) \text{ - for the right wheel} \quad (22)$$

If we assume that the rolling circle of the wheel is a circle centered on the axis of rotation, then the equations for the surface of the wheels are simplified as follows

$$Z_l = \pm\sqrt{Z_l^2(X_o,Y) - X^2} \text{ - for the left wheel;}$$

$$Z_r = \pm\sqrt{Z_r^2(X_o,Y) - X^2} \text{ - for the right wheel.}$$

To solve the problem, we would resort to describing the surface of the wheels in their bottom part, at some interval from $-\Delta X$ to $+\Delta X$.

The surface of the rails is described in the coordinate system $O_\rho\zeta\xi$ - by equations (the rail is considered to be a cylindrical body):

$$\xi_l = \xi_l(\eta) - R_{zpl} / S_{zp} + \xi_{\text{p}l} \text{ - for the left rail;}$$

$$\xi_r = \xi_r(\eta) - R_{zpr} / S_{zp} + \xi_{\text{p}r} \text{ - for the right rail,} \quad (23)$$

where R_{zpl}, R_{zpr} - vertical reactions of the right and the left rail;

S_{zp} - vertical stiffness of the length of rail;

ξ_l, ξ_r - vertical irregularities of the right and the left rail. Taking these factors into account has a significant impact on the calculation results, especially on *tgγ(y)* (in the straight line *tgγ(y)* can vary by -0.02, and in the curve - by -0.12. When the rail is raised in a curve of 150 mm, the angle of inclination of the wheelset, and therefore the change in *tgγ(y)* will be 150/1,580 = 0.095. If we take into account the amplitudes of the irregularities of the rails, the exact values as above are obtained).

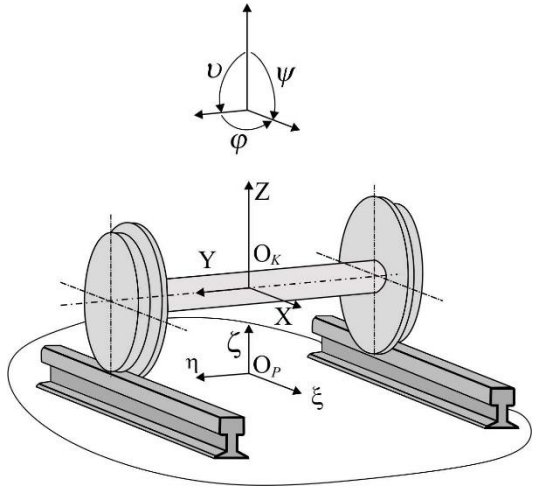

Fig. 23. Design scheme for the wheelset contact with the railway track

Equations (22, 23) are continuous and differentiable. The specific form of the equations depends on the wear of the tires and the rails. In general, the equations describing the surfaces of the right and the left wheel, as well as the left and the right rail may be different.

The task is somewhat simplified, if we consider the same equations describing the profiles of the right and the left rail. Then

$$\xi_l = \xi_l(\eta) \text{ - for the left rail;}$$
$$\xi_r = \xi r(\eta) + \Delta\xi \text{ - for the right rail,} \qquad (24)$$

where $\Delta\xi = (R_{zr} - R_{zl})/c_{zp} + \xi_l - \xi_r$.

Wheelset position in the coordinate system $O_p\zeta\eta\xi$ defined by coordinates ζ_0, η_0, ξ_0 point O_w and three Euler angles φ, ψ and Θ, chosen according to the Krylov method [49] (see Fig. 20).

It is assumed that the coordinate systems move along the railway track at the same speed ($\zeta_0 = 0$) and, in addition, the angle $\psi = 0$. For the convenience of calculations, we adopted the coordinate ζ_0, so the wheelset is "suspended" in the air. Coordinate η_0 and angle φ - are considered preset. Angle Θ is determined in the course of the solution. O_RXYZ и $O_p\zeta\eta\xi$ systems are related by the well-known correlations [49]. They are used to describe in parametric form the surface of the left or the right wheel (respectively) in the coordinate system $O_p\zeta\eta\xi$.

In order to determine the coordinates of the points of contact of the wheels with the rails, we introduce into consideration the functions describing the distance along the axis $O_p\zeta$ between the corresponding points of the wheels and the rails (Fig. 21):

$$H_l = \zeta_l^K - \zeta_l \text{ - for the left side;}$$

$$H_r = \zeta_r^K - \zeta_r \text{ - for the right side.} \qquad (25)$$

The difference between these values gives the value $\rho(\Theta)$.

The problem of finding the contact points is formed as follows:

find angle θ, which for the preset η_0 and φ makes an equation:

$$\min H_r = \min H_l .$$

However, this difference is a function of the angle θ

$$\min H_r - \min H_l = \rho(\theta)$$

Then the problem of finding the points of the initial contact is reduced to solving the equation

$$\rho(\Theta) = 0 \qquad (26)$$

Equation (24) can be solved using one of the approximate methods: - the method of half division. The solution comprises two steps such as separation of the root of the equation, i.e. establishing a clearance $[\Theta_\alpha, \Theta_\beta]$, which contains the root, and the refinement of the approximate roots, i.e. bringing them to a given degree of accuracy.

The result of the solution is the coordinates of the points of initial tangency A and B (Fig. 24) in coordinate systems $O_p\zeta\eta\xi$ and O_pXYZ. Knowing them, it would be easy to determine the values of the radius of the wheel and the angle of arrival to the surface of the wheel and the rail at the point of contact.

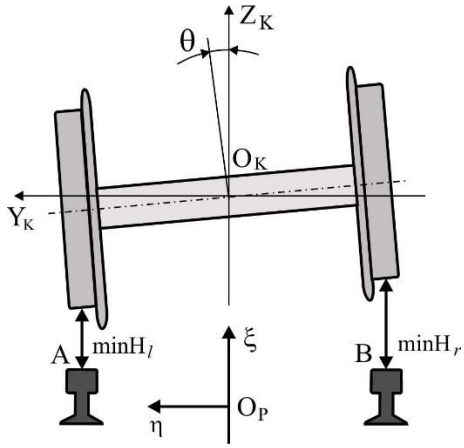

Fig. 24. Calculation model for determining the points of contact of the wheelset with a railway track

According to the described method for determining the dependencies $\Delta R(y)$ and $tg\gamma(y)$ in this work, a numerical experiment was carried out, which yielded the regression equations for various combinations of contacting profiles of the wheels and the rails:

$$\Delta R(y) = (A_1 y + A_2 y^2)(1 - A_3\Delta\xi + A_4\Delta\xi^2);$$

$$tg\gamma(y) = (B_1 + B_2 y^2 + B_3 y^2)(1 + \Delta\xi / 2s);$$

(y[mm], $\Delta\xi$ [m]).

The coefficients of the regression equations for various combinations of surfaces of contacting bodies and the results of calculations are set forth in Table 5 and in Fig. 25, 26.

Here (a) - a new wheel (GOST 11018-87) - a new R65 rail (GOST 8161-75), b) - a worn-out wheel [78] - a new R65 rail, c) - a worn-out wheel [78] - a worn-out rail [78], d) - a new wheel with a unified profile (GOST 11018-87, Fig. 27) - a new R65 rail).

Table 5

Coefficients of regression equations to determine $\Delta R(y)$ and $tg\gamma(y)$

	a)	b)	c)	d)
A_1	0.052381243	0.0049896578 at y>0, 0 at y<0	0.19791 at y>0 0 at y<0	0.00151832
A_2	0.0	0.0731396 at y>0, 0 at y<0	0.068 at y>0 0 at y<0	0.00000048488 at y>0, 0 at y<0
A_3	0.000481	0.00073	0.00057	0.000249
A_4	0.0	0.0267	0.0168	0.0
B_1	0.05	0.0	0.0	0.0
B_2	0.00000648295	0.0	0.0	0.002333 at y>0, 0 at y<0
B_3	0.0	0.0043962 at y>0, 0.000006271 at y<0	0.0034141449 at y>0, - 0.00001046848 at y<0	0.00002452787 at y>0, 0 at y<0

To check the accuracy of the results obtained by the method described above, they were compared with the results of analytical calculations of particular cases of a combination of the contacting surfaces of the wheels and rails. Thus, a numerical method for determining the dependencies $\Delta R(y)$ and $tg\gamma(y)$ has been developed that can be used in virtually any combination of the wheel and the rail surface profiles.

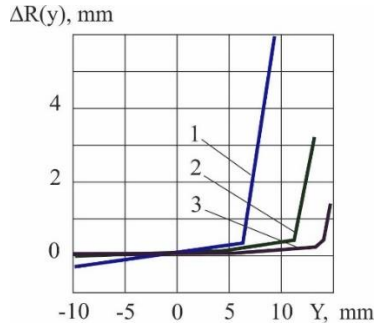

Fig. 25. $\Delta R(y)$ for the profile of the unified wheel in accordance with GOST 11018-87 and the new rail R65; 1 - obtained in [10]; 2 - calculation results in combination with the new R65 rail; 3 - calculation results in combination with a worn-out rail

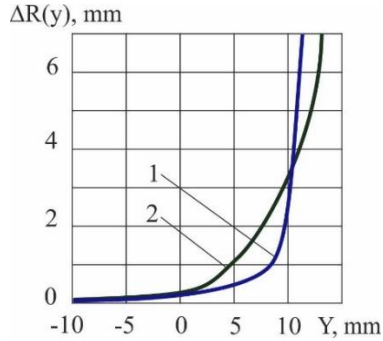

Fig. 26. $\Delta R(y)$ for a worn-out wheel profile; 1 - calculation results in combination with the new R65 rail; 2 - calculation results in combination with a worn-out rail

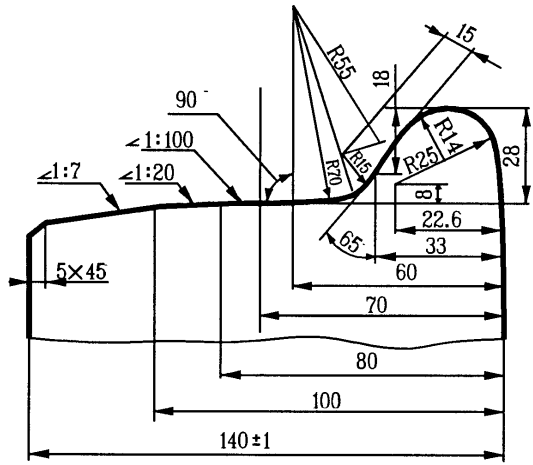

Fig. 27. Unified wheel profile in accordance with GOST 11018-87

4 BENCH EQUIPMENT FOR TESTING THE SPRING SUSPENSION CHARACTERISTICS

4.1. Test bench for axle boxes

The test bench for axle box units and elements of their connection with the frame of a railway rolling stock bogie (Fig. 28, 29) is intended for testing the machinery parts in the conditions as close as possible to real operating conditions, and can be used, in particular, for testing the axle boxes and spring suspension.

The bench frame 1 in Fig. 28 comprises the bars 2 and the beams 3. The shaft 4 with tested axle boxes 5 and 6 at its ends, driven into rotation by an electric motor 7 through clutch 8 and belt drive 9, is installed on the frame 1. The axial load on the axle box 5 and 6 is caused by an axial loading device containing an eccentric mechanism 10, rotated by an electric motor 11 through clutch 12 and belt drive 13. The constant component of the axial load is created by the double-acting hydraulic cylinder 14, the rod of which is connected to the eccentric.

On the beam 3 of the frame 1, hydraulic cylinders 15-18 of the vertical loading mechanism are installed, abutting with the rods against the rolling bearings 19 on the sidewalls 20 and 21, which act on the axle boxes 5 and 6 through the leads 22, shock absorbers 23 and springs 24. Sources of oscillatory loads in the form of electromagnets 25 are mounted between the axle boxes 5 and 6 and the sidewalls 20 and 21. The sides 20 and 21 are rigidly connected to each other by beams 26, forming a movable frame that simulates the frame of the bogie. The longitudinal load mechanism (hydraulic cylinders 27-30 with rollers 31 on the rods) is kinematically connected to the sidewalls 20 and 21 through stops 32 and 33, thereby eliminating any pinching that prevents the sidewalls from moving under the combined action of vertical and longitudinal loads.

Bench tests are carried out as follows.

Depending on the design of the tested axle boxes and the spring suspension elements, the test program, a certain type of load would be applied and their nature would change.

The electric motor 7 rotates the shaft 4. The hydraulic cylinders 15-18 of the vertical loading mechanism transmit forces through the roller bearings 19 to the sidewalls 20 and 21, while the sidewalls load the axle boxes through the connections 22, shock absorbers 23 and springs 24.

The sources 25 of the vibrational load generate the pulsating vertical loads in the tested units and provide a change in their nature and amplitude.

To generate the axial load on the axle box units, turn on the electric motor 11, which, through the clutch 12 and the belt drive 13, rotates the eccentric mechanism 10 that has impact on the shaft 4.

By adjusting the rotational speed of the electric motor, changing the eccentricity of the eccentric piece and its geometry, one would set the frequency of pulsations of the load and change its type. In this case, the constant component of the axial load and its value are generated by the hydraulic cylinder 14.

The axle boxes 5 and 6 and spring suspension elements 22-24 with longitudinal traction load are loaded by the longitudinal loading mechanism when the sidewalls 20 and 21 move, driven by hydraulic cylinders 28 and 30, 27 and 29 in one direction or the other through rollers 31 and stops 32 and 33.

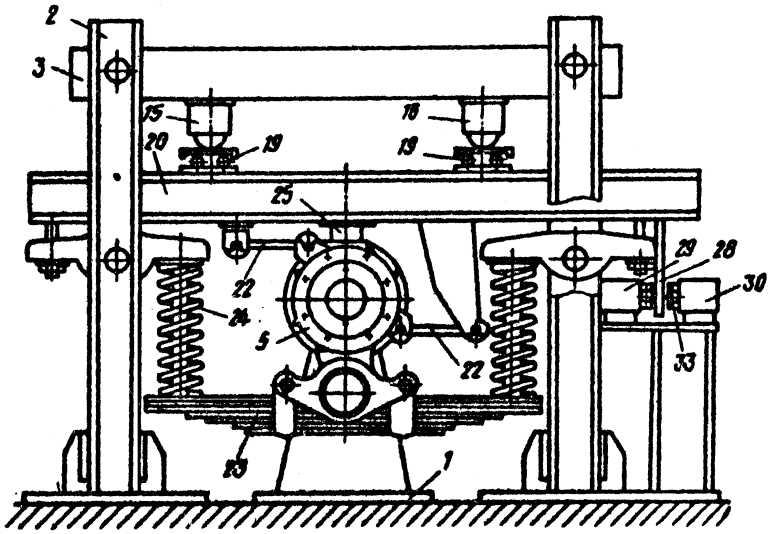

Fig. 28. Axle box unit test bench (side view)

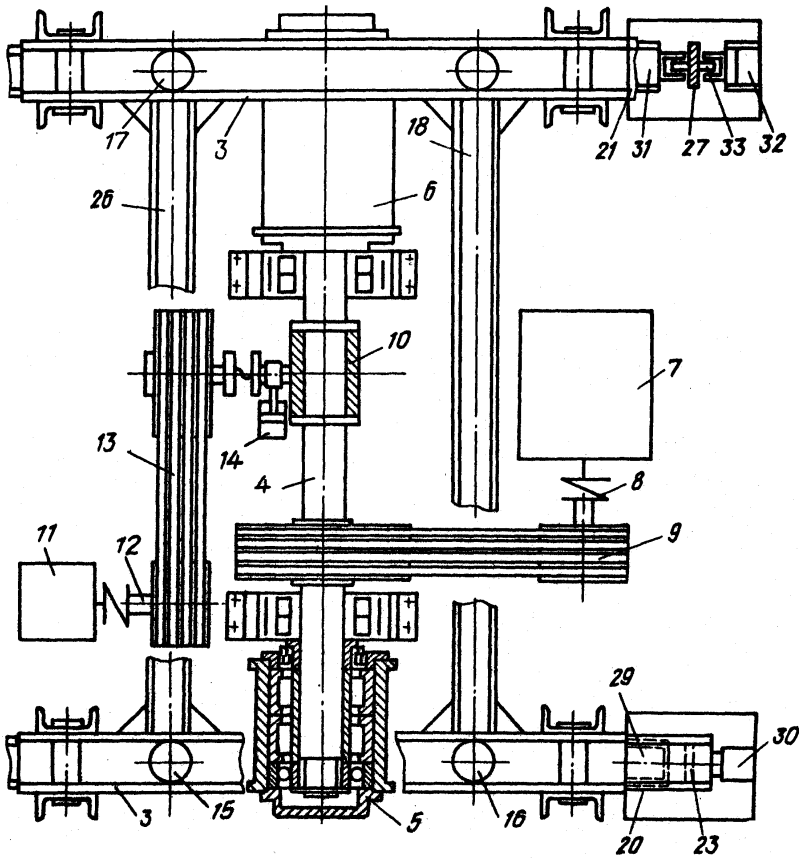

Fig. 29. Axle box units test bench (top view)

4.2. Test bench for vibration dampers

The bench for testing hydraulic vibration dampers (Fig. 30, 31, 32, 33) comprises a prefabricated frame 1, to the upper part of which the upper clamping device 2 is attached, and the support 3 at the bottom part, wherein a vertical rotary bench 4 is installed. Lever 5 is rigidly fixed to the latter. Clamping device 7 is rigidly attached to one of the holes in the plate 6.

The plate 6 is capable of turning in a fixed path around the horizontal axis 8. The tested damper 9 is rigidly fixed in the upper 2 and the bottom 7 clamping devices. The drive elements of the bench are made by known methods and provide a reciprocating movement of the base plate 6, which is converted into reciprocating

movement of the bottom end of the hydraulic vibration damper together with the bottom clamping device 7.

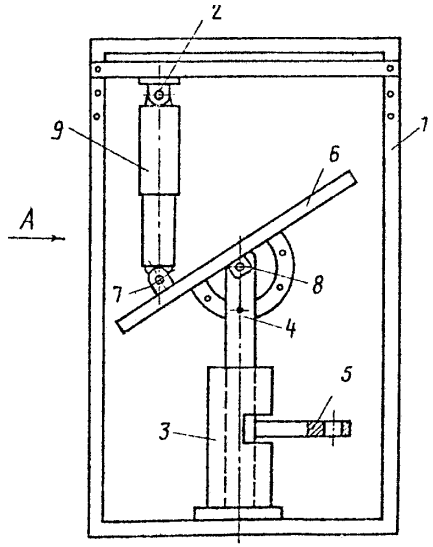

Fig. 30. Test bench for hydraulic vibration dampers

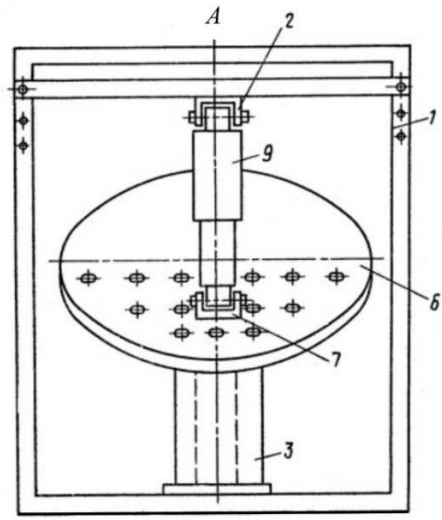

Fig. 31. Test bench for hydraulic vibration dampers (View A)

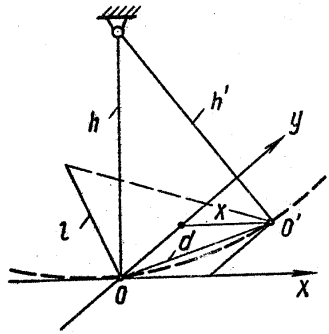

Fig. 32. Calculation diagram of the vibration damper movement (side view)

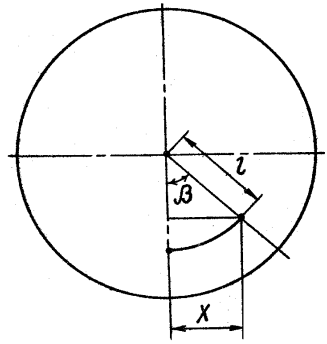

Fig. 33. Calculation diagram of the vibration damper movement (top view)

The test bench works as follows.

Plate 6 rotates relative to the vertical post 4 at a certain angle α, that is determined based on the condition of the necessary working stroke of the vibration damper, and is rigidly fixed in this position. After that, the tested vibration damper 9 is fixed between the upper 2 and the bottom 7 clamping devices. When the bench drive is activated, lever 5 begins the reciprocating motion in horizontal plane, the vertical bench 4 connected to arm 5 transfers the reciprocating motion to plate 6. In this case, the bottom clamping device 7, in conjunction with the bottom head of the vibration damper 9 fixed in it, performs complex spatial cyclic movements relative to the upper head. This motion consists of the movements in three directions along the vertical axis of the damper 9, as well as along and across the axis 8. The travel values in the indicated directions are interrelated and are determined by the

shoulder l of the clamping device 7 installed on the plate 6 and the angle α of the fixed rotation of the plate 6 about the axis 8. Maximum travels in the specified directions at an angle of rotation β of the vertical rotary rack 4 around its axis, depending on the parameters *l* and *y*, are determined by the following dependencies (Fig. 33 - 34.).

$$x=l\sin\beta;\ y=l(1-\cos\beta)\cos\alpha;\ d=\sqrt{h^2+d^2}=\sqrt{h^2+x^2+y^2}$$

With the initial distance between the damper heads *h*, the change in this distance when the rack 4 is rotated through the angle α will be $\Delta h = h' - h$.

The choice of the required ratio between the travels *x, y,* Δh (corresponding to certain operating conditions of a particular type of the rolling stock) is carried out by varying the parameters *l*, *a* and β

Thus, the test bench makes it possible to bring the test conditions closer to real operating conditions due to the fact that the bottom damper head makes a complex movement relative to the upper head. The fact that one common drive is used to create the movements of the bottom damper head in three planes helps to simplify the design of the bench.

43. Test bench for testing the support and the return devices coupling the locomotive body and the bogies

On diesel locomotives 2TE116, 2TE121 of the Holding Company "Luhanskteplovoz", combined rubber-metal supports are installed between the body and the bogies, which provide the elastic separation of the bogies and the body masses and provide lateral travel and angular rotation of the bogies relative to the body.

Such a support contains a roller device with a set of rubber-metal elements (RME) installed on it.

The use of combined supports improves, compared to the rigid support, the dynamic qualities of the locomotive.

Advantages of the rubber parts include their shock-absorbing and vibration-insulating qualities, and the ability to serve as compensator devices when assembling the units. However, modern technology for the manufacture of rubber products is such that the mechanical properties of parts may vary a lot even within a single batch. Tests carried out with the participation of the author showed that the spread of the stiffness parameters of the rubber-metal elements reached 1 kN/m in the vertical direction and 0.02 kN/m in the horizontal direction. The stiffness of

coupling of the body and the bogie frame, which is one of the most important characteristics that determine the dynamic qualities of locomotives, depends on the mechanical properties of rubber parts.

The resistance forces arising with the drift of the bogie and its turn relative to the body have an elastic-dissipative nature. Their value also depends on the design and parameters of the body supports on the bogies (friction in the roller apparatus, the quality of rubber, the number of RME blocks, their geometric dimensions). The values of these parameters determine the horizontal-longitudinal, transverse and vertical stiffness, dissipative forces of connection between the body and the locomotive bogie.

As it follows from the results of theoretical studies, the stability of motion and the characteristics of forced vibrations of the locomotive largely depend on the characteristics of the connection of the second stage of spring suspension. Ultimately, these characteristics determine such parameters of the dynamic properties of the locomotive as the values of horizontal frame forces, smooth travel, etc.

That is why it is very important, even at the design stage, to study the effect of various design changes in the connection of the body with the bogies and the choice of the values at which the dynamic qualities of locomotives would be satisfactory in a given speed range.

Despite the simplicity of the design of the connection between the body and the locomotive bogies with combined rubber-metal supports, it is difficult to theoretically determine their elastic-dissipative characteristics. Oftentimes, the evaluation of elastic connections is made indirectly on the basis of the results of dynamic (running) tests of the locomotive. However, the values of the parameters of the connection between the body and the bogie and the characteristics of the supports can also be determined by bench tests. To this end, the Holding Company "Luhanskteplovoz" has developed and built the benches which make it possible to determine both the characteristics of the supports and the characteristics of the connection between the locomotive body and the bogies in various operating modes.

The bench in Fig. 34 allows full-scale shear testing of supports in the vibration frequency ranging from 0 to 3 Hz and vibration amplitudes from 0 to 0.4 m under harmonic loading in symmetric and asymmetric (with introduction of the static component of deformation) cycles.

The bench features the research object 1, which is a set of electromagnetic relays (RME) under the vertical load that simulates the load from the body by means of device 2 through the metal spacer 3. Device 4 in a steel disk with a rectangular groove allows you to adjust the value of the vibration amplitude in accordance with the specified test conditions. A different value of the vibration amplitude would be obtained by setting the value of the eccentricity of this device, which is set relative to the center of the disk. The disc with the adjusting device 4

is connected to the rod 5 and coupling 6, which allows the vertical axis of symmetry of the test object to be aligned with the axis of symmetry of the facility. The disc is driven into rotation by an adjustable electric drive 7. By adjusting the speed of the DC motor, we change the deformation frequency of the rubber-metal support.

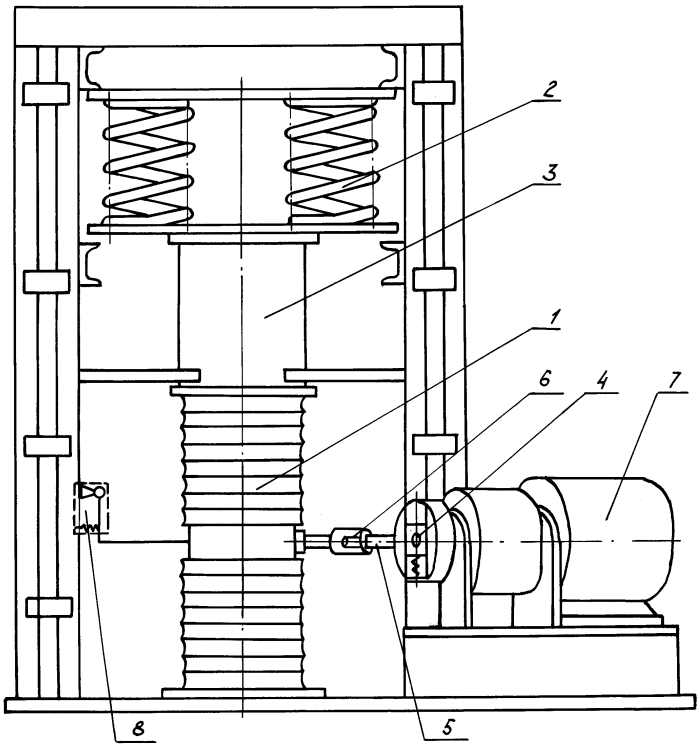

Fig. 34. Bogie test bench

This way, the bench provides an opportunity to evaluate the dynamic properties of RME set depending on both the deformation frequency and the vibration amplitude. Wire gages are pasted to sleeve 6 to record the values of the elastic force that causes deformation of the rubber specimen. The registration of deformations is carried out by a beam deflection meter 8.

By feeding the signals of the beam deflection meter and the sensor for measuring the elastic restoring force of the test specimen to the loop oscilloscope, we register the travels and the corresponding forces.

A minor modernization of the bench would allow testing the combined supports with a roller apparatus and an RME set on it. The bench allows simulating the forces arising in the support during the drift and the sweep of the bogie relative to the locomotive body.

Experimental studies to determine the resistance forces and the moments arising in the support-restoring devices during the drift and the sweep of the bogie are carried out on a four-support bench.

Fig. 35. shows a general view of the described bench. Fig. 36 provides the top view.

The bench contains a fixed base 1 with rolling bearings 2 installed on it, on which a bottom frame 3 is located, simulating a bogie. On the fixed base 1, there are struts 4 with lateral motion mechanisms 8, connected by means of the strain gage rods 6 with the bottom movable frame 3, and struts 7 with angular motion mechanisms 8, connected by means of the strain gage rods 9 with the upper movable frame 10 imitating the body.

Between the upper and the bottom movable frames 3 and 10 simulating the bogie and the body, there is a test interface between the body and the bogie comprising of supports 11 and pivot assembly 12. Rolling bearings 15 are located between the upper movable frame 10 and the vertical additional loading devices 13 mounted in the U-shaped frames 14. Springs 17 are located between the crossbars 16 of the frames 14 and the vertical loading devices 13.

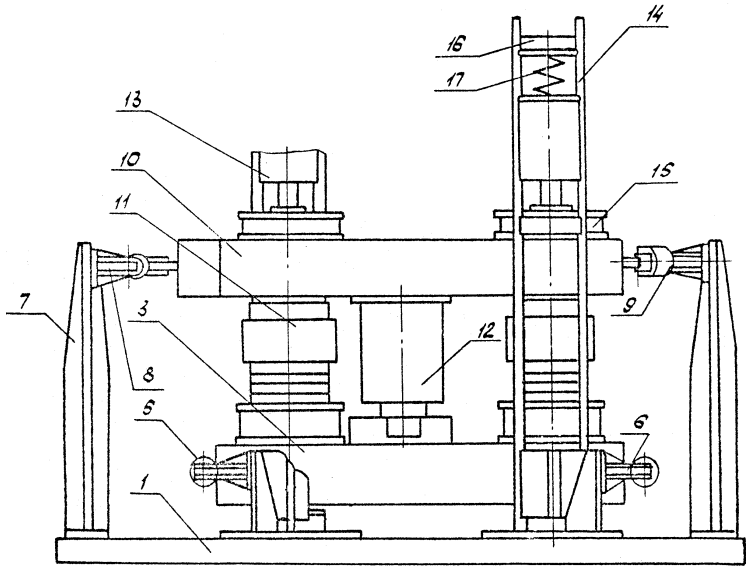

Fig. 35. Test bench for testing the connection between the body and bogies

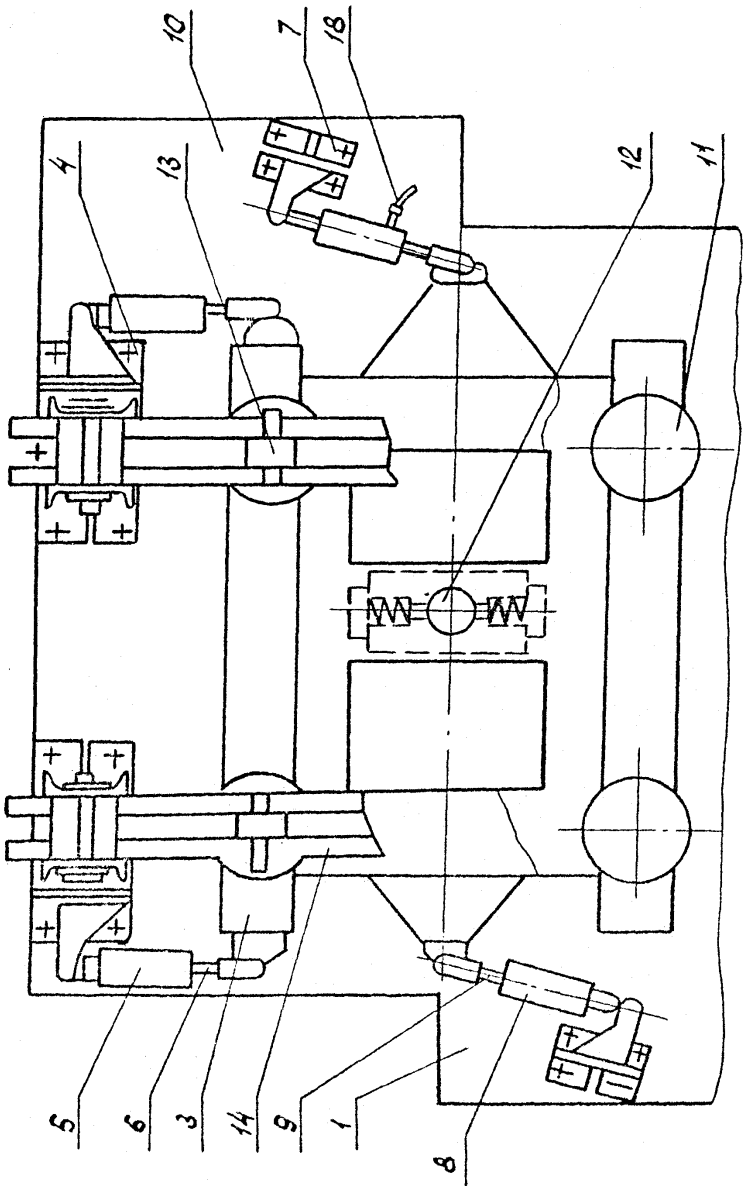

Fig. 36. Test bench for testing the connection between the body and bogies (top view)

Devices for vertical loading, shear forces and angular travels are driven by the hydraulic system of the bench (see Fig. 37).

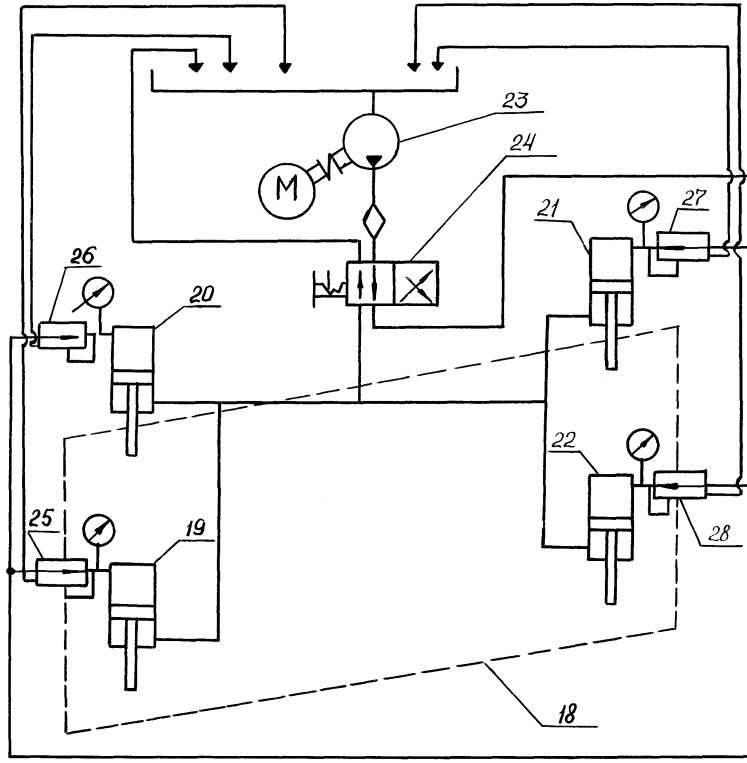

Fig. 37. Hydraulic system of the bench

The device for vertical loading of the bench is made in the form of paralleled hydraulic cylinders 10, 20, 21, 22 connected by a pump 23 through control valve 24. Each hydraulic cylinder has a pressure reducing valve 25, 26, 27, 28.

The upper and the bottom movable frames 10 and 3 that simulate the body and the bogie have a system of holes allowing changing the coordinates of the facility of the tested interface between the locomotive body and the bogie in the longitudinal and the transverse directions.

The bench works as follows. In accordance with the test program and the design of the tested interface between the locomotive body and the bogie, the object of study is out under a vertical load through the supply of the working fluid by

pump 23, through the control valve 24 and the hydraulic cylinders 19, 20, 21, 22 of the vertical loading device 13.

When testing the couplings with a symmetrical arrangement of supports relative to the pivot, the pressure reducing valves 25, 26, 27, 28 are turned off and equal pressure is maintained in all hydraulic cylinders.

When testing the interfaces of the locomotive body with the bogie having an asymmetrical arrangement of supports relative to the kingpin, the working fluid is supplied by the pump 23 through the control valve 24 to the hydraulic cylinders 19, 20, 21, 22, creating a vertical load on the tested supports 11; by adjusting the pressure reducing valves 25, 26, 27, 28, you can equalize the load on the supports by changing the pressure in the hydraulic cylinders.

If you need to simulate:

- dynamic fit of the locomotive into the curved track sections accompanied by the motion of the locomotive body and a change in the load on the support, the pressure reducing valves 25, 26, or 26, 27 will change the load on the supports located on both sides of the longitudinal axis of the bogie at equal distances by adjusting the pressures in hydraulic cylinders 19, 22 or 20, 21.
- the galloping the bogie and generation of the traction force, the pressure reducing valves 25, 26 or 27, 28 release the pressure in the hydraulic cylinders 19, 20 or 21, 22, creating a difference in the loading of the front and the rear supports in the direction of the bogie motion.

To capture a picture of the processes that occur in coupling of the body with the bogie, the change in the location of individual points of the carriage is recorded by sensors. Linear and angular travels of the elements of the tested supports and units of the bench are equalized with the help of the beam deflection meters. Forces with a relative travel of the upper and the bottom frames are measured with the help of dynamometric inserts that are fitted with temperature sensors. Signals from the sensors of deflection meters and inserts are amplified by the TUP12 amplifier installed in the circuit and recorded by the N-004 oscilloscope. Sensors are to be calibrated before the commencement of testing.

By using of these benches, you will be able to define the properties of the body with the bogies as soon as the design stage, checking the effectiveness of the improvements made, identifying their shortcomings. You will also be able to clarify a number of provisions in the calculations of vehicles and reduce the amount of expensive dynamic tests.

5 MATHEMATICAL MODEL OF THE LOCOMOTIVE MOTION

Taking into account the results obtained in the previous sections, the following prerequisites were laid as the basis for constructing a mathematical model of a six-axle locomotive motion:

1. Spatial vibrations are considered.
2. The motion of two sections of a six-axle locomotive on a track section of an arbitrary outline in the plan is studied.
3. All bodies of the system (locomotive body, bogie frames, electric traction motors (ETM), wheelsets and tires) are assumed to be absolutely rigid.
4. Nonlinearities in the axle boxes during the lateral runs of the wheelsets, in pivot assemblies when carrying bogies, in body supports on a bogie with the rocking vehicle, were taken into account.
5. The action of friction elements in the axle box spring suspension is considered.
6. The force of resistance to the motion of the locomotive and train is taken into account.
7. The calculations are carried out when the locomotive is moving in the coasting, traction and braking mode.
8. The adhesion force is determined separately for each wheel, depending on the vehicle speed, the sliding speed of contacting bodies, the vertical load, frictional state, the wheel and the rail profiles, and their relative position. Various models of frictional interaction are used to represent the adhesion force between the wheel and the rail (4, 15, 38).
9. The longitudinal speed of the locomotive is determined in the process of integrating the differential equations of motion and no restrictions are imposed on its value.
10. The track is considered in the form of discrete inertial beams of infinite length, lying on an elastic-dissipative [76] or elastic-viscous [14, 16] base, under the action of vertical and lateral horizontal forces applied at the points of contact between the wheels and rails. Dissipativity is taken into account by dry friction forces [76], viscosity is taken into account by the drag coefficient ε_x [14, 16]. The reduced track mass is assumed to be constant [14, 15, 16]. The path stiffness values are taken according to [14, 15, 76].
11. The tire and the rail have arbitrary profiles.
12. Friction of the wheel flange on the rail is taken into account when choosing a clearance in the railway track.
13. Electrodynamic processes during the motor operation are taken into account.
14. Longitudinal vibrations of the train train are taken into account during the motion.
15. The torsional stiffness of the wheelset axle is taken into account.

16. Fig. 38 shows a general view of the considered model (one section). symbols of the movement of all bodies of the system are summarized in Table 6.

Table 6

Symbols for the travels of all bodies comprising the system

	Travel					
	linear, along the axes			angular, relative to the axes		
	OX	*OY*	*OZ*	*OX*	*OY*	*OZ*
Body	x_b	y_b	z_b	θ_b	φ_b	ψ_b
Bogie frame		y_{Tk}	z_{Tk}	θ_{Tk}	φ_{Tk}	ψ_{Tk}
Wheelsets	x_{wi}	y_{wi}	z_{wi}	θ_{wi}	φ_{wi}	ψ_{wii}
Motor						ψ_{tmi}
Armature						ψ_{ai}
Rails at the contact points		y_{pij}	z_{pij}			

Here k = 1, 2 - bogie number;

i = 1,2 ... 6 - the number of the wheelset in the locomotive; indices (j = 1) right and left, (j = 2) sides in the direction of travel, in addition, m = 1, 2, 3, 4 are used to indicate the number of the body support on the bogie.

The following restrictions are imposed on the movement of the bodies in the system:

1. While in motion, the wheel does not come off the rail surface. Then the vertical travel of the rail lines are as follows

$$Z_{pij} = Z_{rimij} + \delta R_{ij}$$

where Z_{rimij} - vertical travel of the tires,

δR_{ij} - changes in the rolling radius of the wheel. For linear profile of the wheels

$$\delta R_{ij} = (-1)^{j+1} \lambda y_{rimij},$$

$$\delta R_{ij} = f_1(y_{rimij}).$$

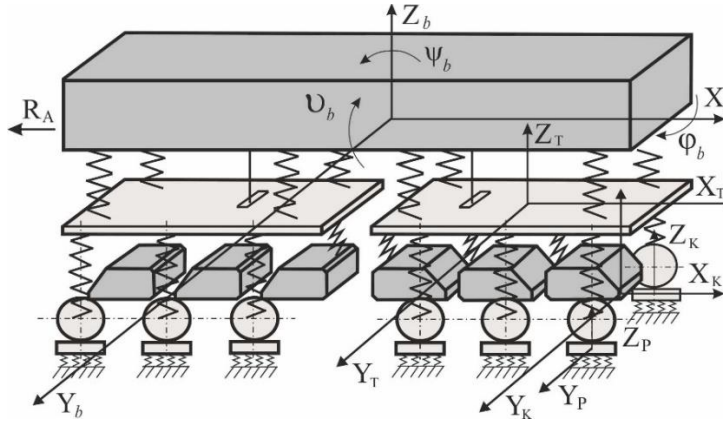

Fig. 38. Design scheme of spatial vibrations of a 6-axle locomotive

Specific kind of function f_1 for various combinations of wheel and rail profiles are set forth in Section 5.

2. The connection between the body and the bogies in the longitudinal direction is absolutely rigid, i.e. $x_b = x_{T1} = x_{T2}$.
3. With axial support, the traction motor is rigidly connected to the axle of the wheelset, except for the rotation about the axis OY.
4. The traction motor armature in the housing can only rotate about the axis OY, the traction drive is rigid.
5. The travel of the tracks occurs in two directions - along the axes OY and OZ.
6. The wheelset is assumed to be an absolutely rigid body; only the torsional stiffness of the axle is taken into account.

There are 21 bodies in the system (body, two bogies, six traction motors, six traction motor armatures, six wheelsets) each of them has six degrees of freedom. The rails under each wheel have two degrees of freedom (a discrete model of the track is considered). Taking into account the available joints, the system has 21·6+6+12·2-12·1-2·1-6·5-6·6=76 degrees of freedom. Its behavior is described by differential equations of the second order. In addition, to determine the traction moment, the currents in the traction motor circuits are found, which means 6 more generalized coordinates. The second section of locomotives has the same number of connections. When modeling the train composition for each car, only longitudinal vibrations are considered, and since the number of carriages N can be arbitrary, then N generalized coordinates are added.

5.1. Testing the mathematical model of locomotive motion, analysis of the influence of the choice of the adhesion model on the calculation results

To check the adequacy of the mathematical model of locomotive movement and to compare the influence of different adhesion models on the results of traction and dynamic calculations, a number of problems were considered:

- coasting of the locomotive;
- locomotive moving in traction mode on the site;
- hitting an oil slick when the locomotive is moving in traction mode at maximum power;
- locomotive starting off with a train of carriages.

The results of calculations of the dynamic processes obtained in solving the first problem were tested by comparison with the results of the running tests of diesel locomotives 2TE-116 No. 517 and No. 1012, carried out by the department of dynamic and strength tests of the HC "Luhanskteplovoz" [69] and the All-Russian Scientific Research Diesel Locomotive Institute (Kolomna) [39]. Test results are summarized in Table 7 and 8.

Table 7

Comparison of the calculation results and the experimental data by the values of the coefficients of horizontal and vertical dynamics

Experiment [69]				Calculation			
v, m/s	16.7	22.2	27.8	Model	16.7	22.2	27.8
$\kappa_{\partial 2}$	0.07	0.1	0.14	(17)	0.085	0.111	0.143
				(8)	0.133	0.128	0.174
				(6)	0.141	0.130	0.157
$\kappa_{\partial 6}$	0.15	0.16	0.18		0.155	0.167	0.183

Table 8

Comparison of the maximum frame forces (R_{bu}, kN) obtained during the trial trips of 2TE-116 locomotives and the estimates of mathematical expectations of their maximum values

wheelset number								
	1		3		4		6	
v, m/s	experiment	calculation	experiment	calculation	experiment	calculation	experiment	calculation
11.1	1) 7.5	4) 7.31	1) 11.0	4) 3.82	1) 8.0	4) 8.92	1) 8.0	4) 9.88
	2) --	5) 12.10	2) --	5) 10.60	2) --	5) 17.26	2) --	5) 18.77
	3) --	6) 15.75	3) --	6) 17.56	3) --	6) 17.95	3) --	6) 19.03
16.7	1) 10.0	4) 11.85	1) 14.0	4) 7.47	1) 11.0	4) 11.06	1) 14.0	4) 14.68
	2) 11.0	5) 17.88	2) 11.0	5) 16.53	2) 9.0	5) 18.85	2) 8.0	5) 23.94
	3) 15.0	6) 23.40	3) 12.0	6) 17.55	3) 13.0	6) 20.84	3) 12.0	6) 25.45

22.2	1) 13.0	4) 12.75	1) 18.0	4) 15.49	1) 14.0	4) 17.57	1) 22.0	4) 20.00
	2) 15.0	5) 13.34	2) 17.0	5) 17.93	2) 13.0	5) 14.72	2) 18.0	5) 22.91
	3) 14.0	6) 17.5	3) 17.0	6) 21.50	3) 14.0	6) 18.61	3) 22.0	6) 23.45
25.0	1) 14.9	4) 18.26	1) 21.0	4) 17.93	1) 16.0	4) 20.56	1) 27.0	4) 22.39
	2) --	5) 22.83	2) --	5) 25.29	2) --	5) 23.36	2) --	5) 27.94
	3) --	6) 27.05	3) --	6) 27.78	3) --	6) 27.18	3) --	6) 29.71
27.8	1) 22.0	4) 20.41	1) 24.0	4) 24.83	1) 17.0	4) 21.75	1) 32.0	4) 25.71
	2) 16.0	5) 22.48	2) 13.0	5) 25.60	2) 14.0	5) 21.96	2) 14.0	5) 27.94
	3) 18.0	6) 28.13	3) 17.0	6) 28.08	3) 19.0	6) 27.62	3) 30.0	6) 29.71
33.3	1) --	4) 25.24	1) --	4) 22.00	1) --	4) 17.86	1) --	4) 24.13
	2) 13.0	5) 22.51	2) 9.0	5) 19.25	2) 13.0	5) 13.32	2) 12.0	5) 24.15
	3) 17.0	6) 19.53	3) 12.0	6) 20.71	3) 15.0	6) 13.23	3) 14.0	6) 22.25

1) - [39], 2) - [69], forward, 3) - [69], reverse (numbering of the wheelsets in the direction of the travel of the locomotive), 4) - [24] , 5) - [40] , 6) - [83]

Analysis of the results in Table 7, 8, in Fig. 39, 40 demonstrates their satisfactory convergence with the experimental data on the values of frame forces, coefficients of vertical and horizontal dynamics, vertical and horizontal accelerations of bogies and the body. Moreover, the closest to the experimental data are the estimates obtained using the adhesion model (20).

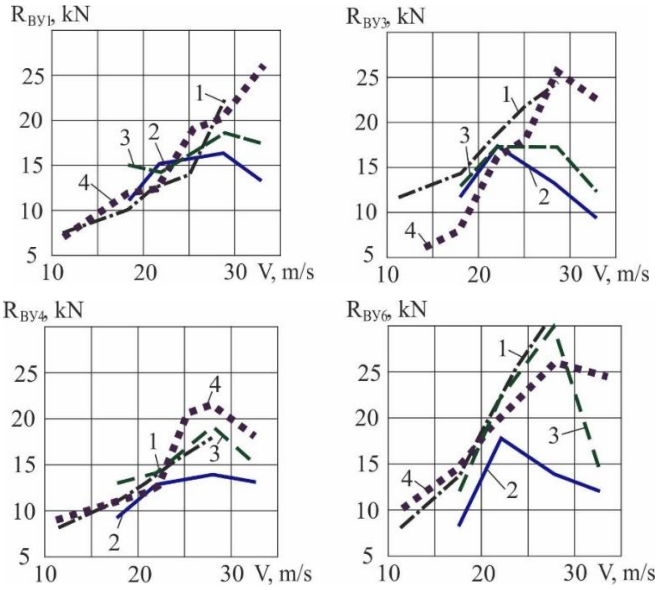

Fig. 39. Maximum frame forces obtained during the running tests of the 2TE116 locomotive (1 - [39], 2,3 - [69]) and the results of the estimates of mathematical expectations of their maximum values - 4 (model [20]) when coasting

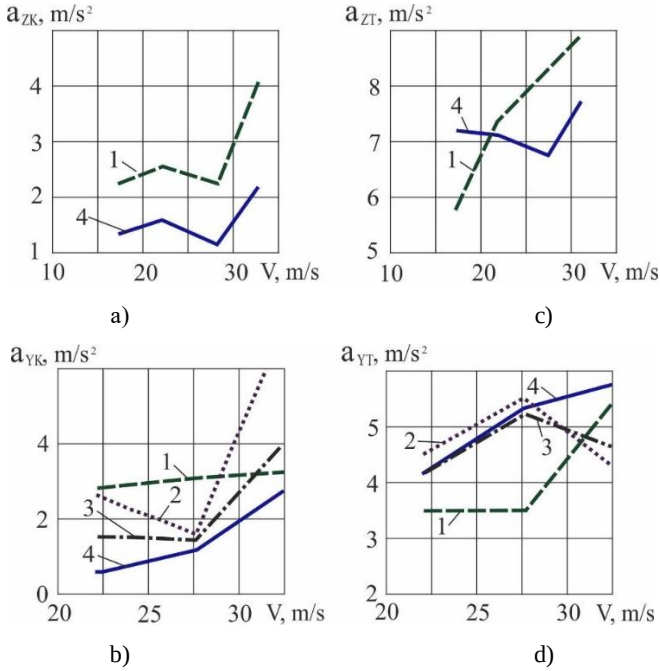

Fig. 40. Dependence of the change in maximum acceleration on the coasting speed of the locomotive; a) - vertical, b) - horizontal bodies in the area of the tie box, c) - vertical, d) - horizontal bogies, 1 - according to [69], 2 - model [83], 3 - model (46), 4 - model [24]

It should be noted that the results of calculations of dynamic processes in the vertical plane when simulating the coasting do not depend on the choice of the adhesion model. The same result was obtained in [71, 72]. This is due to the fact that F_{sc} acts in a horizontal plane and does not directly affect the vertical vibrations, whereas the vertical forces mostly depend on the locomotive parameters and the track in a vertical plane.

The results of solution to the problem of the locomotive motion in traction mode on the site are set forth in Table 9 and 10.

Table 9

Values of the average total longitudinal adhesion forces [kN] along the track section at *v*=10 m/s and *v*=20 m/s, at maximum power, maximum adhesion of 0.3

Model	New profiles		Worn out	
	10 m/s	20 m/s	10 m/s	20 m/s
(6)	164.286	52.225	164.487	52.174
(8)	164.475	52.211	164.435	52.011
(17)	163.590	51.545	163.520	52.161

Table 10

Values of the average total longitudinal adhesion forces [kN] along the track section at *v*=10 m/s and maximum adhesion of 0.15 and *v*=20 m/s and maximum adhesion of 0.1, at maximum power

Model	New profiles		Worn out	
	10 m/s	20 m/s	10 m/s	20 m/s
(6)	164.390	52.262	164.480	52.192
(8)	164.360	52.233	164.405	52.169
(17)	157.550	49.520	156.960	49.169

The results of the traction parameters estimates when using different adhesion models differ to a greater extent than the dynamic ones. This is due to the fact that as a result of a different approach to solving the problem of the interaction of the locomotive wheel with the rail, the models take into account the factors influencing the adhesion process in different ways.

The values of the average total longitudinal adhesion forces along the section and the coefficient of use of adhesion weight under good contact conditions (clean, dry rails, μ=0,3) for all models do not differ (value η=0.941 at v=10 m/s and η=0.98 at v=20 m/s), since they are the result of the action of the same tractive moments and the magnitudes of the forces F_{xad} do not reach the adhesion limit (Table 10).

At the same time, the amplitude of changes in the adhesion force will be different for each specific model. Fig. 41, 42, 43 demonstrate the change in the vertical load and the adhesion force depending on the distance traveled for the first wheelset of the locomotive in traction mode and using different adhesion models. The oscillation amplitudes F_{ad} are observed in model (20). For models [40, 83], the amplitudes of oscillation of the tractive force of one wheelset were 2-3 kN, for the adhesion model [20] - 5-6 kN, for the entire locomotive - 10-20 and 30-40 kN, respectively.

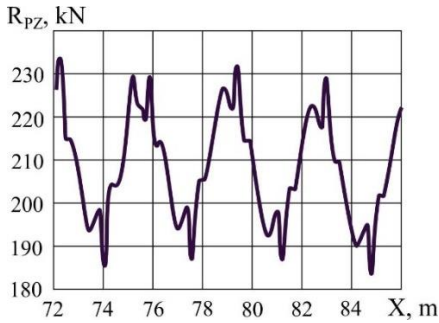

Fig. 41. Change in the vertical load from the first wheelset on the rails with the locomotive motion at v=10 m/s

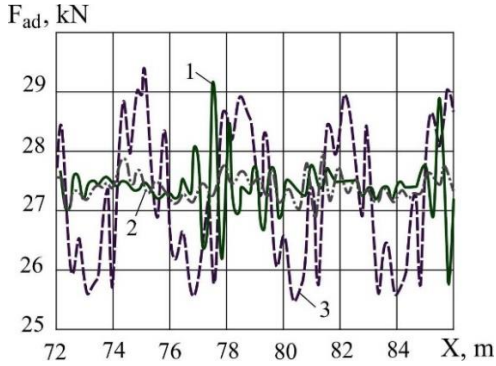

Fig. 42. Changes in the adhesion force of the first wheelset with the locomotive motion at v=10 m/s and maximum adhesion μ= 0.3, - model [83], 2 - [40], 3 - [24]

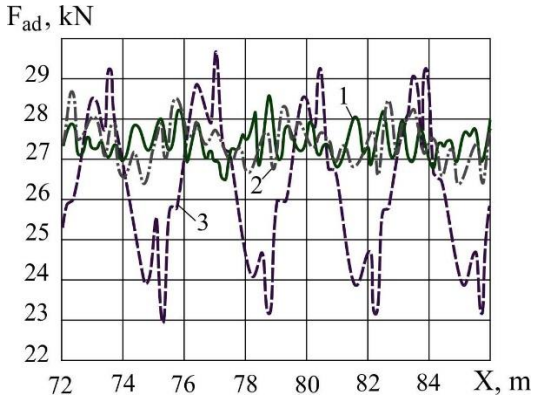

Fig. 43. Changes in the adhesion force of the first wheelset with the locomotive motion at v=10 m/s and maximum adhesion
μ=0.15, 1 - model [83], 2 - [40], 3 - [24]

The amplitude of the change in the tractive force of the entire locomotive, according to [56], was 40-60 kN (Fig. 44). [80] provides the results of measuring the tractive force of one wheelset of an electric locomotive VL10a with an axial load of 24 tons when in traction mode (Fig. 45). The amplitude of oscillations in the tractive force was 8-12 kN with the adhesion coefficient of 0.34-0.37. Comparison of these results shows that the results of the estimates using the adhesion model (20) are the closest to the experimental data in terms of the amplitude of oscillation of the tractive force.

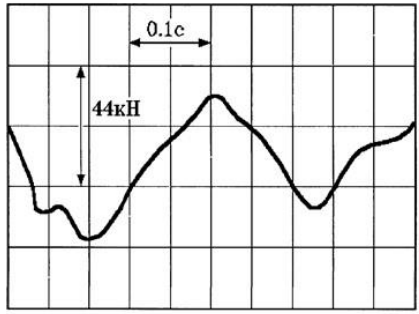

Fig. 44. Oscillograph chart of the tractive force of a locomotive with a support-axle drive [56]

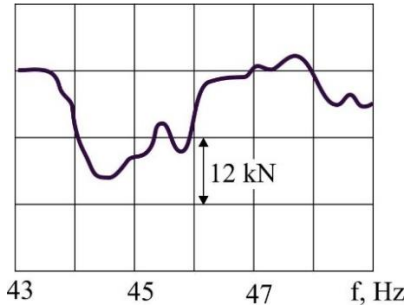

Fig. 45. Curve of the tractive force change from one axis of VL80a electric locomotive during the acceleration [80]

Due to the biggest vibration amplitude, the smallest value of mean F_{ad} along the travel segment with deteriorating friction contact conditions is observed when using model (20) (Table 10).

To this effect, at the maximum adhesion of 0.15, v=10 m/s, M_t=14.5 kNm per wheel pair, the total average tractive force for the section in (17) was smaller by 4.6% or 7.5 kN for the new wheel and rail profiles, and 4.2% or 6.85 kN for worn-out profiles than in other adhesion models.

At maximum adhesion of 0.1, v=20 m/s, M_t=4.5 kNm per wheelset, the decrease in tractive force in model [20] was 5%, or 2.7 kN, for the new and 4.8%, or 2.5 kN, for worn-out profiles compared to models [40, 83].

η=0.941 at v=10 m/s for models [40, 83] and η=0.95 (20), at v=20 m/s η=0.98 for all models. Increase in the value η for model (20) is explained by the fact that

the first (it is also the limiting) wheelset is at the adhesion limit, the level of decrease in its adhesion force is greater, and the adhesion coefficient is smaller than for the entire locomotive.

The results of the solution to the problem of locomotive movement in traction mode at maximum power at v=10 m/s along the oil slick (i.e., a sharp decrease in frictional properties on the track section from μ=0.3 to μ=0.1, followed by the recovery thereof) are shown in Fig. 46, 47.

One can see that the estimates of the locomotive motion in different adhesion models are not the same.

For a short slick (< 30 m) passed over a relatively short time when no visible slipping occurs, the slipping stops for any model as soon as the frictional conditions are restored (Fig. 46).

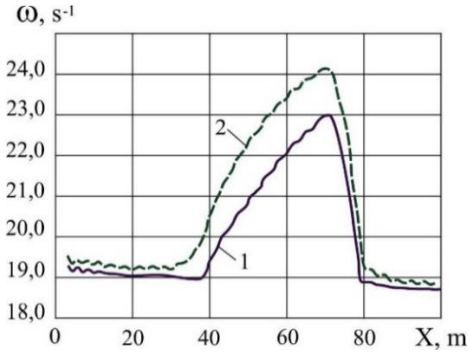

Fig. 46. Change in the angular speed of the first wheelset when the locomotive travels over an oil slick 30 m long (1 - for model [40], 2 - for model [24])

In the event of a long-term presence of a locomotive on an oil slick (over 50 m long), when skidding develops over a long period of time, skidding does not stop when the frictional conditions are restored under model [20], but with model [83], the skidding does stop (Fig. 47).

This is because there is no descending branch on the adhesion characteristic in model [40], and upon restoration of the frictional conditions of the contact, if the tractive force does not exceed the adhesion limit in the new conditions, a decrease in the slip always occurs and the adhesion is restored (Fig. 48, a). Here, respectively, are the points: 1 - the moment when the oil slick ends, 2 - restoration of frictional conditions (μ=0.3), 3 - the end of the slipping process. In this case, when switching to a new adhesion characteristic (μ=0.3) forces do not reach the limit (points 1, 2, 3).

According to the model (20), the adhesion characteristics have a descending branch. Therefore, if the slipping process has developed deeply enough (Fig. 48,

b, points 1', 2'), then the restoration of frictional conditions does not result in the cessation of slipping, because on the new traction characteristic (μ=0.3) point 2' is still on the descending branch under skidding conditions and this process can be stopped only by dumping of the load, i.e. tractive forces, and this is exactly how they solve this problem in reality.

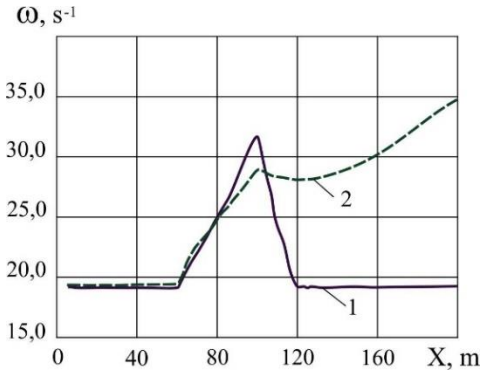

Fig. 47. Change in the angular speed of the first wheelset when the locomotive travels over an oil slick 50 m long (1 - for model [40], 2 - for model [24])

If, with the improvement of frictional conditions on the new characteristic, the forces do not reach the adhesion limit (Fig. 48, b, points 1, 2, 3), the skidding can stop without the dumping of the load.

When solving the problem of the starting of a locomotive with a train of carriages from the spot, a train of 20 carriages, 80 tons each, located on the site, was simulated. Resistance of the train of carriages when starting off and in the initial period of movement was determined in accordance with [8, 9] $W_{mp}=42W/(29+s)$, where s - path from the starting point, km. When starting off, the limitation of the power of the locomotive by the current of the motors was simulated.

When using model (20) the locomotive starts off at the maximum adhesion of 0.375, which is quite consistent with the real conditions.

For the adhesion model [83], in contrast to the model [20], it was not possible to simulate the starting process. The break into slipping occurred even at the maximum adhesion of 0.6, which does not correspond to reality. This can be explained by the fact that at very low speeds, the longitudinal oscillations of the train and the locomotive cause small (however considerably above the critical) absolute values of the relative slip on the adhesion characteristic and the locomotive goes into the slipping process. Therefore, as it follows from the review of the literature dealing with the study of the processes occurring during the operation of a locomotive in the traction mode, including slipping and starting, the authors use for calculations

the experimental characteristics of adhesion [51, 63, 70] or introduce the "coefficient of angular stiffness of the elastic coupling of the wheel to the rail in the direction longitudinal to the axis of the track"[62], while theoretical models of adhesion are more often used to calculate the vehicle motion in coasting mode [15, 40, 52, etc.].

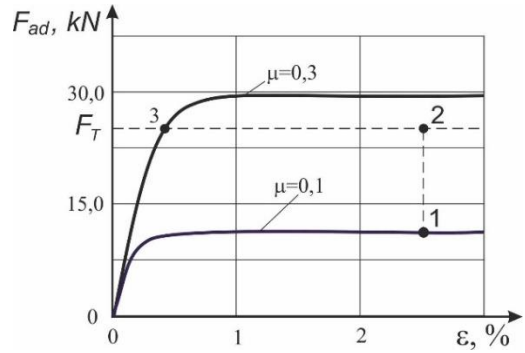

a)

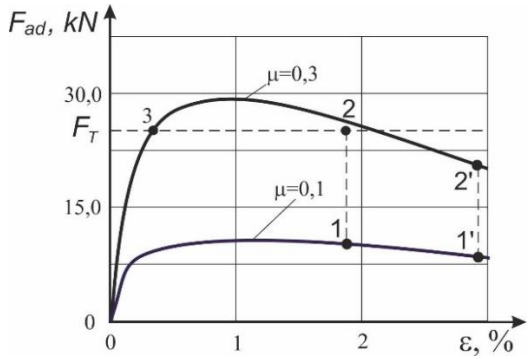

b)

Fig. 48. Influence of the adhesion characteristics on the development of the skidding process (a) - model [40], b) - model [24])

There is an obvious collision here, since the physics of the process of frictional interaction between the wheel and the rail does not depend on the mode of the locomotive motion, at least in the literature known to the author it is not indicated that the adhesion in the traction mode differs from the adhesion during the coasting. The adhesion process shall be simulated in the same way in both traction and dynamic estimates.

According to the data obtained from solving the problem of the locomotive starting from rest under poor frictional conditions of the wheel-to-rail contact

(μ=0.2), the locomotive went into slipping. At the same time, the process of development of frictional self-oscillations of the wheelset axle at 30-35 Hz was observed (Fig. 49). The value of the dynamic moment on the traction motor shaft was 4.73 kNm with traction moment before the commencement of slipping 8.11 kNm.

Similar processes were recorded when testing the operation of the 2TE121 diesel locomotive (Fig. 50) and the VL81, ChS4 electric locomotives in the starting mode under poor frictional conditions and the development of the slipping process [34, 37, 36, 51, 62].

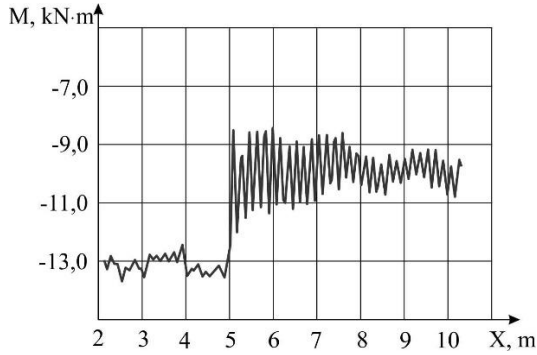

Fig. 49. Moment on the axle of a wheelset of a locomotive (calculation)

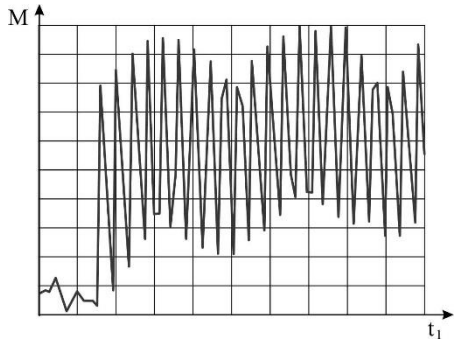

Fig. 50. Moment on the axle of a wheelset of a diesel locomotive 2TE121 [34,62]

In [36, 37], testing a diesel locomotive TEP10 No. 333 in the slipping mode at the start off, produced slipping with the development of oscillatory processes. In this case, the value of the dynamic moment on the traction motor shaft was 4.15 kNm with a traction moment before the slipping commenced - 8.65 kNm.

Comparison of these results once again confirms the reliability of the developed model.

5.2. Influence of the tractive force of a locomotive on the results of calculation of the dynamic processes in the "vehicle-track" system

To assess the influence of the traction moment and frictional conditions of wheel-to-rail contact on the dynamics of locomotive motion, a series of calculations was carried out for two traveling speeds: at v=10 m/s, μ is taken at 0.3 and 0.15; at v=20 m/s, μ - 0.3 and 0.1. Minimum values of μ are taken from the estimates of the adhesion force close to the adhesion limit but not exceeding it.

Mathematical expectations of the maximum frame, lateral and transversal adhesion forces for combinations of the new wheel profiles with worn-out rails and worn-out wheels with worn-out rails are set forth in Table 11, 12 and in Fig. 51, 52.

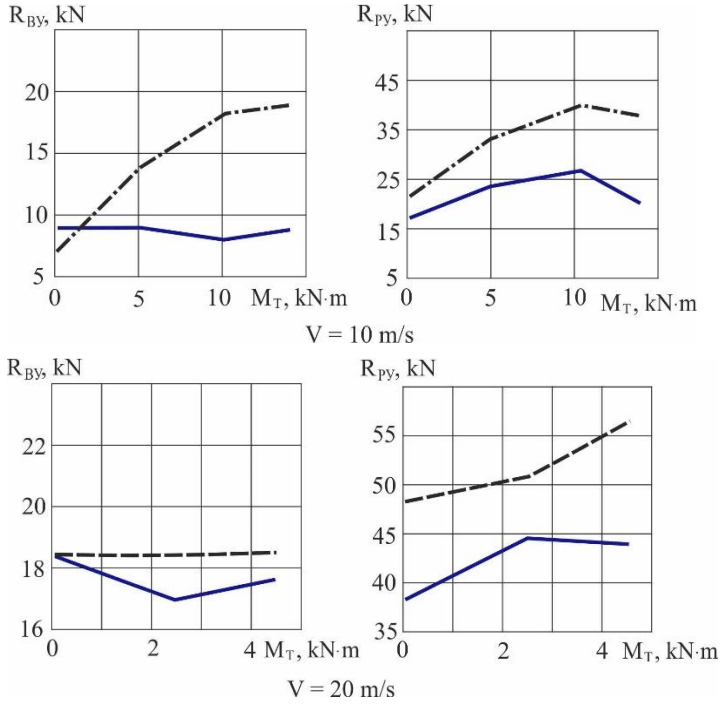

Fig. 51. Changes in the maximum frame and lateral forces depending on the tractive moment for new wheel and rail profiles:
—— μ=0.3; —·—·—· μ=0.1; - - - - - - μ=0.15

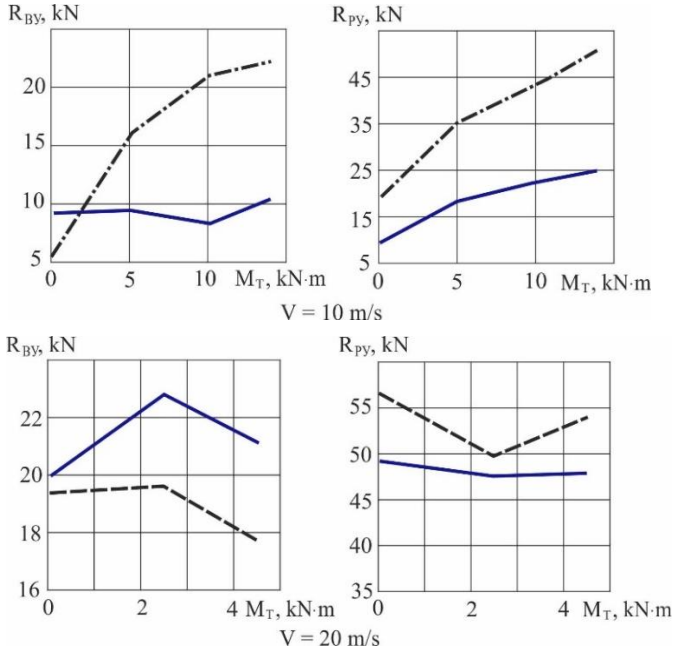

Fig. 52. Changes in the maximum frame and lateral forces depending on the tractive moment for worn-out wheel and rail profiles:
—— μ=0.3; — · — · — - μ=0.1; - - - - - - μ=0.15

Table 11

Estimates of mathematical expectations of the maximum frame, lateral and transversal adhesion forces (calculation) for the new wheel and rail profiles [kN]

			wheelset number							
			1	3	4	6	1	3	4	6
v, m/s	μ		Traction				Coasting			
10	0.3	$R_{бу}$	3.87	6.08	8.35	9.32	5.23	3.07	8.42	9.33
		F_y	9.93	4.28	9.45	6.81	9.82	2.25	6.98	7.48
		$R_{ру}$	21.81	14.42	18.60	16.53	18.43	7.46	11.87	9.00
10	0.15	$R_{бу}$	12.40	11.84	12.26	19.64	6.86	2.46	5.68	7.00
		F_y	2.27	2.27	2.60	3.22	2.26	1.45	2.62	2.49
		$R_{ру}$	21.00	14.90	36.32	37.87	11.82	9.09	11.34	22.18
20	0.3	$R_{бу}$	12.59	12.79	13.39	17.76	12.37	13.23	14.05	18.42
		F_y	13.51	10.34	16.29	13.02	11.01	10.01	14.58	13.05
		$R_{ру}$	43.53	36.66	37.10	32.38	32.83	37.90	35.27	36.81
20	0.1	$R_{бу}$	15.96	17.15	15.68	18.53	14.03	15.83	15.20	18.47
		F_y	2.15	2.70	2.89	3.22	2.26	3.34	2.95	3.66
		$R_{ру}$	55.47	47.47	55.05	48.74	40.94	47.95	40.80	45.72

Table 12

Estimates of mathematical expectations of the maximum frame, lateral and transversal adhesion forces (calculation) for worn-out wheel and rail profiles

wheelset number										
			1	3	4	6	1	3	4	6
v, m/s	μ		Traction				Coasting			
10	0.3	$R_{бy}$	7.68	6.64	6.76	11.23	8.80	7.67	8.74	9.50
		F_y	10.23	4.47	8.51	8.84	7.58	5.91	7.00	7.25
		R_{py}	25.49	7.96	18.52	17.53	9.76	9.18	9.19	8.72
10	0.15	$R_{бy}$	14.63	10.68	16.71	22.35	4.40	3.70	4.94	5.88
		F_y	2.70	2.72	3.90	5.13	1.48	1.37	2.02	4.52
		R_{py}	28.74	19.94	34.92	51.44	9.40	6.71	7.74	19.31
20	0.3	$R_{бy}$	12.76	16.38	15.11	21.13	14.64	16.69	16.74	20.00
		F_y	17.05	14.85	15.78	19.39	15.06	15.22	14.89	18.52
		R_{py}	47.59	42.06	46.62	31.59	47.73	37.88	42.56	49.19
20	0.1	$R_{бy}$	13.85	12.86	17.61	17.81	15.11	16.19	15.43	19.56
		F_y	4.03	2.48	3.46	4.25	3.65	5.59	4.27	6.10
		R_{py}	23.33	35.29	53.31	41.99	47.73	42.44	41.68	56.65

As one can see from Table 11, 12 and Fig. 51, 52, in most of the calculated driving modes, when traction is applied to the wheelset, an increase in the maximum values of frame (2.8) and lateral (1.7 times) forces is observed.

This effect does not occur when the adhesion force does not reach the maximum possible value determined by the frictional conditions.

For example, at v=10 m/s, the increase in R_{BY} and R_{PY} is much bigger than at v=20 m/s. This is due to the fact that M_t at v=10 m/s reaches 14-14.5 kNm per wheelset, versus 4-4.5 kNm at v=20 m/s. At v= 20 m/s, for worn-out profiles of wheels and rails, no increase in R_{BY} and R_{PY} is observed.

To combine the new wheel profiles with the new rails at v= 10 m/s and μ=0.3 with an increase in M_t from 0 to 14.5 kNm per wheelset, the maximum frame forces change little, lateral forces increase by 45%, with μ=0.15 the maximum frame forces increase by 170%, lateral forces - by 80%. For worn-out wheels and rails at the same travel speed at μ=0.3, frame forces increase by 18%, lateral forces - by 160%. At μ=0.15, the frame forces increase by 280%, lateral forces - 170%.

The level of frame and lateral forces in the traction mode at v= 10 m/s, especially for worn-out profiles of wheels and rails, is comparable to R_{BY} and R_{PY} at v= 20 m/s.

A similar effect of the increase in R_{PY} (by 140%) occurs when frictional conditions deteriorate in the coasting mode and, to an even greater extent, in the traction mode (an increase in R_{BY} reaches 110% and in R_{PY} -100%).

At v=10 m/s, M_t =14.5 kNm and μ decreasing from 0.3 to 0.15 for the combination of the new wheel profiles with the new rails, the maximum values of frame forces grow by 110%, lateral forces - by 70%, for worn-out wheels and rails, frame forces increase by 100%, and lateral forces - also by 100%.

At v= 20 m/s, M_t = 4.5 kNm and μ decreasing from 0.3 to 0.1 for new profiles of wheels and rails, an increase in frame forces does not occur, lateral forces increased by 27%, for worn-out wheels and rails the increase in frame forces was 19%, for lateral forces - 12%.

According to the analysis of the results of the locomotive motion calculations, there is a significant influence of the tractive force and frictional conditions in the contact between the wheel and the rail on the dynamic processes in the transverse direction (Table 11, 12, Fig. 51, 52).

These results have been further confirmed experimentally. Destabilizing effect of the traction torque on the locomotive motion in the horizontal plane was registered in experimental work carried out at the Department of Locomotive Engineering of the East Ukrainian State University and during the test runs of the TEM2 locomotive No. 7024 by the All-Russian Research Diesel Locomotive Institute [18, 19, 47].

The results herein are of considerable interest in determining the dynamic qualities of a locomotive, since the tractive force can have a noticeable destabilizing effect on the process of its movement.

Let us compare these data with the results of other studies on the influence of the traction moment on the rail vehicle movement.

In [18, 19, 38, 44, 48, 61, 60], the effect of the traction moment on the nature of the locomotive motion or its wheelset is noted. However, opinions on the influence of the latter are divided. For example, the traction moment allegedly stabilizes the movement of the vehicle in the straight section of the track in [44], while destabilizing the same in [18, 25, 38, 47, 48,].

Let us try to sort this out.

The locomotive motion and generation of the tractive force occurs by way of the wheelsets rolling on a railway track. Therefore, we should consider the results of calculating the single wheelset motion in the stopping and the traction modes [26]. In addition, this approach makes the task easier, since the wheelset-track system is much simpler than the locomotive-track system.

The wheelset interacts with the railway track in the horizontal plane by means of adhesion forces in the contact between the wheel and the rail, inertia, gravitational stiffness and the interaction of the wheel flange with the rail head at the moment of their contact (Fig. 53). Their action determines the nature of the wheelset motion.

The adhesion force is the reaction of the rail to the external influences and is by its nature a friction force [45], i.e. the reaction of resistance to the movement of

the contacting bodies. This kind of movement (sliding) is the result of the traction moment and the kinematics of the wheelset motion:

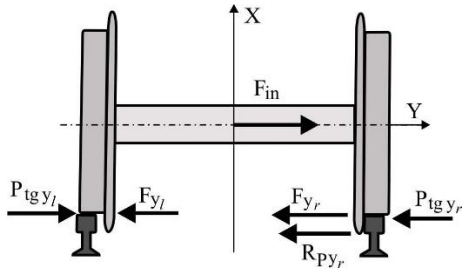

Fig. 53. Diagram of the interaction forces of a wheelset with the railway track

$$\vec{F}_{ad} = \vec{F}_m + \vec{F}_\kappa$$

where $\vec{F}_m$ - the component of the adhesion force caused by the traction moment;

$\vec{F}_\kappa$ - the kinematics of the movement (wobbling).

$\vec{F}_{ad}$ - broken down into longitudinal and transverse components. At first approximation, one can record

$$F_{ad} = \sqrt{F_{adx}^2 + F_{ady}^2}\ . \qquad (27)$$

F_m - can also be broken down into longitudinal and transverse components (Fig. 55).

F_{tx} - - performs the useful work of moving the wheelset in the longitudinal direction.

F_{ty} - always directed along the wobble angle ($F_{ty} = F_t \sin\varphi$) and destabilizes the motion, since it acts in phase with the transverse speed of motion (φ and $\vec{F}_{ad} = \vec{F}_m + \vec{F}_\kappa$ change in one phase). Therefore, a slight (1-2%) decrease in L is observed with an increase in M_t (ranging from 0 to 1025 kNm) [22]

With further increase in M_t , L begins to grow. This is due to the effect of mutual influence of F_{adx} on F_{ady} and it happens as follows.

With the growing M_t, F_{adx} will increase, because M_t is always located in the vertical plane oriented in the direction of the wheelset motion. With F_{ady}, things are more complicated. As it follows from (27)

$$F_{ady} = \sqrt{F_{ad}^2 - F_{adx}^2}$$

Since F_{ad} can be regarded as a constant in certain conditions, F_{ady} will go down with the increase in F_{adx}.

In addition, due to the nonlinear nature of the adhesion, an increase in the adhesion force by the same amount but in different parts will cause an uneven (mounting) growth in ε. Then, generation of the same F_{yad} with an increase in the tractive moment will require a greater ε_y (Fig. 55, $F_{ady1} = F_{ady2}$, $\varepsilon_{y1} < \varepsilon_{y2}$). Consequently, M_t, while increasing the F_{xad}, will increase the amount of transverse slip required to maintain F_{ady}.

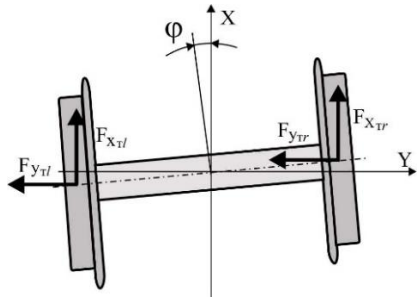

Fig. 54. Pattern of the action of tractive forces on the wheelset

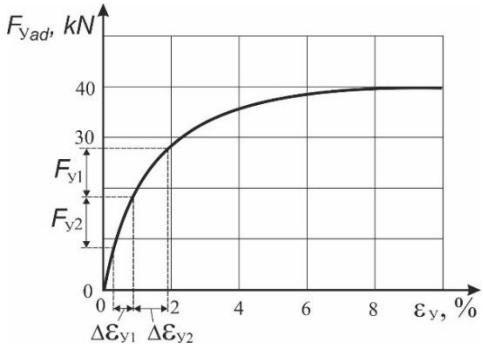

Fig. 55. Influence of the changing adhesion force on the values of transverse skid

Therefore, with an increase in the tractive moment, there is a decrease in the transverse forces of adhesion and, consequently, in the forces of resistance to the transverse motion. As a result, lateral forces increase (up to 90% depending on the speed and magnitude of M_t, same as the rails displacement (100%) and the time of contact with the ridge of the rail head wheel (80%) for new profiles of wheels and rails. The wavelength of the wobble drops at first [22] and then increases due to a significant reduction in F_{cuy} and the increasing time of contact between the ridge

and the rail [22], i. e. lateral adhesion forces can no longer keep the wheelset in the track.

For worn-out profiles, the increase in the wobble wavelength [22] is observed at the M_m, lower than for the new profiles. This is due to the fact that the wobble frequency, the transverse speed of the wheelset in the railway track, and, consequently, the value of F_{ady} in this case, is larger (for example, at v= 10 m/s, the amplitude of changes in F_{ady} is 8.1 versus 1.52 kN for the new wheel and rail profiles) and the influence of F_{adx} on F_{ady} occurs at a lower M_t. The movement of the wheelset is largely determined by the forces of gravitational stiffness, which in this case are greater than for the new profiles (their amplitude is 12.02 against 0.084 kN).

Experimentally [18, 19, 17, 48, 82, 88] (Fig. 56) the influence of F_x on F_y and ε_x on ε_y was established.

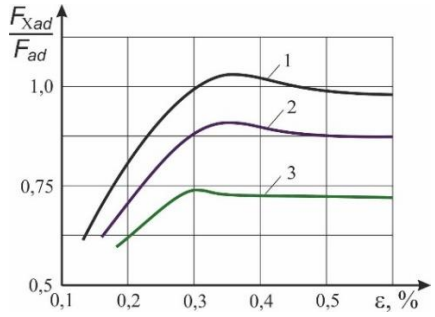

a)

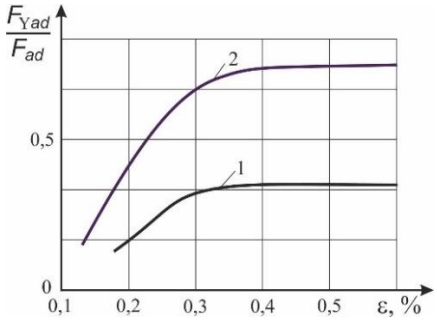

b)

Fig. 56. The influence of the values of longitudinal and transverse skid on the adhesion properties: a) - dependence of the relative adhesion force on the longitudinal skid at varying values of the transverse skid: 1 - $\varepsilon_y/\varepsilon_x$=0; 2 - $\varepsilon_y/\varepsilon_x$=0.5; $\varepsilon_y/\varepsilon_x$=1;
b) - the dependence of the relative transverse force on the longitudinal skid at varying values of the transverse skid: 1 - *Ey/Ex* =0.5; *Ey/Ex*=1

The movement of a locomotive in traction and coasting modes gives the same qualitative picture as the calculations of the movement of a single wheelset, but there are some peculiarities. The first feature is associated with the action of the transverse components of the tractive force. The wobble angles of a wheelset in a carriage are smaller than that of a single one. Therefore, the values of F_{my} (Fig. 54) are small and have no noticeable impact on the locomotive motion. The second feature is the presence of disturbances coming from the track in both the vertical and horizontal planes. Their impact appears to be as follows. M_t increases F_{adx} and decreases F_{ady}, i.e. the forces of resistance to displacement in the transverse direction, therefore, the kinetic energy of the movement of the elements of the "wheel-to-rail" system in this direction caused by the disturbances is dampened at a smaller extent. This also increases the contact time of the wheel flange with the rail head. And the longer the ridge is in contact with the rail, the more disturbances from the track will be transmitted to the vehicle in the horizontal plane. In addition, at the moment of contact of the flange with the rail head, when choosing a clearance in the track, the nature of the interaction between the wheel and the rail changes. It is carried out not only by means of F_{ady} but also by the elastic forces of the rail length, the stiffness of which is very high, which at this moment causes an increase in the interaction forces in the "vehicle-track" system.

The tractive force, due to its influence on F_{ady}, can significantly intensify the dynamic processes.

The following patterns are observed in the calculation results.

1. Depending on the magnitude of the tractive force and frictional conditions, M_t may have a considerable destabilizing effect on the nature of the locomotive motion, since it causes an increase in the dynamic forces (frame forces by 180-280% max, and lateral forces - by 80-170%).
2. Deterioration of the frictional conditions has the same effect on the processes occurring during the locomotive motion, as does the increase in the tractive torque.
3. The wear of the profile of the wheel rim causes an increase in dynamic forces during the movement of the vehicle. In most calculated driving modes, frame and lateral forces for worn-out wheels are 40-70% higher than for the new ones.

5.3. Influence of dynamic processes on generation of the tractive force during the locomotive motion

A lot of works indicate that the dynamic processes occurring during the locomotive motion have a significant impact on generation of the tractive force [18, 19, 28, 29, 51, 56, etc.].

[51, 56] show the dependence of the average tractive force generated by a locomotive without going into slipping on a track section on the type and amplitudes of vertical disturbances. No similar assessment of the influence of horizontal disturbances on the magnitude of the tractive force is available.

Therefore, this work involved calculations and estimates of the influence of oscillations in both the vertical and horizontal planes on the traction of the locomotive.

To simplify the task, the extent of the tractive force was estimated depending on the stiffness of the axle box stage of the spring suspension in the vertical and horizontal directions, since the level of dynamic forces in the locomotive directly depends on the stiffness of the spring suspension elements.

Calculations were carried out for one section of a 2TE116 diesel locomotive moving in the traction mode at v= 10 m/s and μ=0.1. Vertical stiffness of the axle box stage S_{BZ} varied from 377 to 1508 kN/m, the transverse (S_{BY}) - from 4000 to 16000 kN/m per axle unit.

The results of calculations of the tractive force averaged over the section of the track, generated by the locomotive without going into skid, and the dynamic forces in the "locomotive-track" system are provided in Fig. 57, 58, 59.

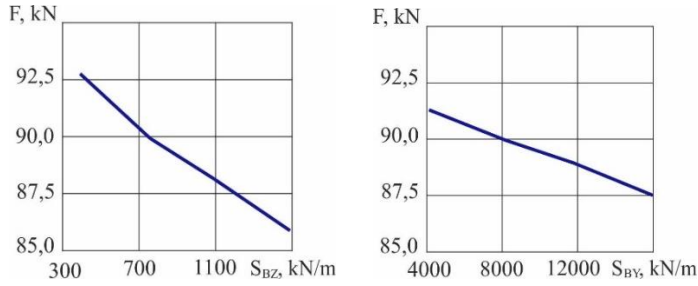

a) b)

Fig. 57. Change in the average tractive force in the area depending on:
a) – the vertical stiffness of the axle box spring suspension;
b) – the transverse stiffness of the axle box spring suspension

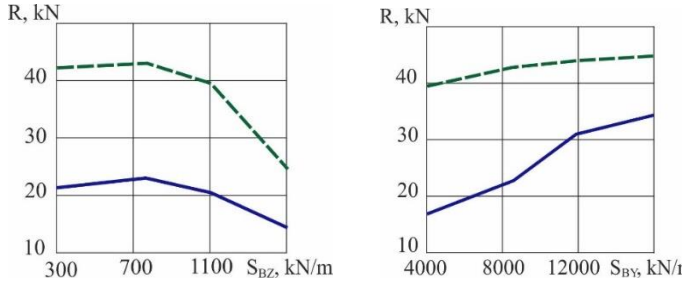

a) b)

Fig. 58. Change in the maximum dynamic forces in the "locomotive-track" system depending on:
a) – the vertical stiffness of the axle box spring suspension;
b) – the transverse stiffness of the axle box spring suspension

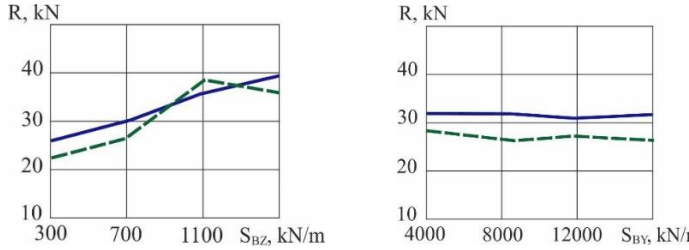

a) b)

Fig. 59. Change in the maximum dynamic forces in the "locomotive-track" system depending on:
a) – the vertical stiffness of the axle box spring suspension;
b) – the transverse stiffness of the axle box spring suspension;
——— R_{bz}, - - - - R_{rz} redistribution of vertical loads on wheelsets during traction and braking in order to align them [29, 56]

As one can see from Fig. 58, 59, 60, the increase in $жс_{бz}$ caused the increase of the maximum vertical dynamic forces in the axle box spring suspension by 54.6%, and from wheelsets to track - by 55.5%. R_{BY} and R_{RY} decreased by 35.1 and 41.2%, respectively. The average tractive force decreased by 7.67%.

The increase in S_{BY} led to the increase in frame and lateral forces by 100 and 13.15%, respectively, while the average tractive force decreased by 4.52%. The values of the maximum vertical dynamic forces remained practically unchanged.

The calculation results show that the dynamic processes occurring during the locomotive motion have a significant impact on generation of the tractive force.

BIBLIOGRAPHY

1. Auto-oscillations and motion stability of the rail vehicles / *Yu.V. Dyomin, L.A. Dlugach, M.L. Korotenko, O.M. Markova* - K.: Nauk. dumka, 1984. - -159 p.
2. *Agliulin Kh.N.* Frictional slippage of surfaces with rolling friction: Abstract of thesis. dis. ... Ph.D. In Engineering. - M., 1971. -17 p.
3. *Adler Yu.P., Markova E.V., Granovsky Yu.V.* Planning the experiment to find the optimum conditions. M.: Science, 1976. - 280 p.
4. *Alexandrov A.I.* Solution of spatial contact problems on stationary rolling of elastic bodies // In collection: Load capacity and reliability of mechanical systems. K.: Nauk. dumka, 1987. - p. 115-121.
5. *Aleksandrov A.I., Boborykin V.G., Melnikov S.D.* On one iterative process of solving the problem of interaction of elastic bodies // Applied math and mechanics. - M.: Science, 1986. - v. 50. - Print 2. - p. 328-331.
6. *Alexandrov A.I., Grachyov V.F.* Application of the finite element method in the problem of the contact between the wheel and the rail // Problems of dynamics and strength of a railway train: Intercollegiate collection of studies - Dnepropetrovsk, 1981. - Print. 220/28. - p. 116-122.
7. *Anikeev I.P.* System for detecting skidding for a diesel locomotive with traction motors of independent excitation // Academic tr. Moscow Institute of Railroad Transport Engineering. - 1979. - Print. 627. - p. 45-52.
8. *Astakhov P.N.* Resistance to the movement of the railway rolling stock. - M.: Transport, 1966. - 178 p.
9. *Astakhov P.N., Grebenyuk P.T., Skvortsova A.I.* Reference book on traction calculations. - M.: Transport, 1973. - 256 p.
10. *Bazilevich Yu.N., Chernyak A.Yu.* Determination of the change in the radius of the wheel at the point of contact with the rail // Complicated mechanical vibrations systems. - K.: Naukova Dumka, 1990. - p. 59-64.
11. *Blokhin E.P., Khachapuridze N.M., Polyakov V.A.* On the influence of spatial oscillations of a train carriage moving along a path of arbitrary shape on the adhesion coefficients of its locomotives // Thes. report All-Union. scientific - tech. conf. "Creation of high-power locomotives and raising their technical level." - Voroshilovgrad, 1981. - p. 111-114.
12. *Bowden F.P., Tabor D.* Friction and lubrication of solids. - M.: Mechanical engineering, 1968. - 543 p.
13. *Burchak G.P.* Oscillations of unsprung mass moving on a rail with random geometric unevenness // Research of dynamics and strength of electric rolling stock / M.: MIIT. - 1971. - Print. 374. - p. 194-212.
14. *Verigo M.F., Kogan A.Ya.* Interaction of the track and the rolling stock /. *M.F. Verigo.* - M.: Transport, 1986. - 559 p.
15. *Vershinsky S.V., Danilov V.N., Khusidov V.D.* Car dynamics: A textbook for higher educational institutions of the railway transport *S.V.* Vershinsky - 3rd ed., revised and modified - M.: Transport, 1991. - 360 p.
16. *Garg V.K., Dukkipati R.V.* Rolling stock dynamics. Translated from English by A.V. Popov / eds. *N.A. Pankin.* - M.: Transport, 1988. - 391 p.

17. *Golubenko A.L., Tkachenko V.P., Turchin V.P.* Results of the experimental studies of the rubberized wheel prototypes / Voroshilovgrad: VMSI, 1988. - 201 p.
18. *A.L. Golubenko* Wheel-to-rail adhesion. - K.: VIPOL, 1993. - 448 p.
19. *A.L. Golubenko* Enhancing the traction properties of diesel locomotives by improving the mechanical components of the vehicle affecting the adhesion of the wheels to the rails. Thesis of the Doctor of Engineering: 05.22.07 - M., - 1986. - 588 p.
20. *Golubenko A.L., Kostyukevich A.I., Dyadyushkin A.P.* Experimental study of the frictional properties of railway rails // Design and manufacture of transport machinery. - Kharkiv: Osnova. -1993. - Print 22. - p. 8-12.
21. *Golubenko A.L., Kramar N.M.* Methods for accounting for forces in the zone of contact between a wheel and a rail. Problems of transport engineering. - Tula: TPI, 1981. - p. 84-90.
22. *Golubenko A.L., Gorbunov N.I., Vivdenko Yu.G.* Influence of tractive force on the dynamic processes during the motion of a rail vehicle / Problems of transport and ways to solve them / Thesis report International scientific and technical conf., - Kyiv, 1994. - p. 107.
23. *Golubenko A.L., Kostyukevich A.I.* Algorithm for solving the contact problem with an arbitrary position of the wheelset relative to the railway track // Design and manufacture of transport machinery. - Kharkiv: Vyshcha shkola, 1989. - Print. 21. - p. 33-37.
24. *Golubenko A.L., Kostyukevich A.I., Gorbunov N.I., Kashura A.L., Polishchuk V.A.* Solution of the contact problem of frictional interaction of a wheel pair with a railway track. Dep. at the State Scientific and Technical Library of Ukraine 12.12.96. No. 2395-Uk-96.
25. *Golubenko A.L., Kostyukevich A.I., Kashura A.L.* Assessment of traction and dynamic qualities of a locomotive at the design stage // Thesis report at the intl. conf. "State and prospects of the development of locomotive building". - Novocherkassk. -1994. - p. 106-108.
26. *Golubenko A.L., Kostyukevich A.I., Kashura A.L.* Applicability of various models of adhesion in solving problems of dynamics // Thesis report of the IV intl. scientific and technical conf. "Problems of development of the locomotive building".- Crimea. - 1993. - p. 4
27. *Golubenko A.L., Kostyukevich A.I., Kashura A.L., Gorbunov N.I., Vivdenko Yu.G.* Comprehensive assessment of traction and dynamic qualities of locomotives at the design stage. Dep. at the State Scientific and Technical Library of Ukraine on 02.21.96. No. 590-Uk-96.
28. *Golubenko A.L., Tkachenko V.P.* Influence of dynamic factors on the process of adhesion and wear in the contact of locomotive wheels with rails / Voroshilovgr. machine building in-t. - Voroshilovgrad., 1983. - 28 p. - Dep. in UkrNIINTI N 393Uk-D84.
29. *Gorbunov N.I.* Improving the traction qualities of diesel locomotives by improving the elastic coupling of bogies: Abstract of Thesis, Ph.D. Engineering: 05.22.07. - DIIT, Dnepropetrovsk, 1987. - 18 p.
30. *Gorbunov N.I., Kostyukevich A.I., Kashura A.L.* Modeling the adhesion force when solving the problems of wheel motion on the rail. Bulletin of the East Ukrainian national university - Luhansk: VUGU. -2001. - Print 7(41). - p.
31. *Danovich V.D., Reidemeister A.G.* Determination of the change in the radius of the rolling circle of the wheel taking into account the lateral rolling and wobbling of the

wheelset // Technical maintenance and use of rolling stock. Dnepropetrovsk. - 1994. - p. 23-27.
32. *Dashevsky E.A., Shnyrev G.D.* The electronics weighing. M.: Knowledge, 1976. - 64 p.
33. Dynamics of the steady motion of locomotives in curves / Ed. *Kutsenko S.M.* - Kharkov: Vyshcha shkola, 1975. - 132 p.
34. Dynamic and strength tests of the traction drive of wheelsets of the diesel locomotive 2TE121-002B on the tracks of the Ministry of Railways: Research report (final) / PKTI; OIP N 20-81; Voroshilovgrad, 1981. - 149 p.
35. *Y. Yevdokimov* Application of modeling methods in solving problems of friction and wear in machines // Tr. RIIZT. - 1972. - Print. 84. - p. 3-62
36. *A.S. Yevstratov* Locomotive running gear. - M.: Mechanical engineering, 1987. - 136 p.
37. *A.S. Yevstratov* Dynamic loads of the locomotive running gear from vibrations of unsprung parts and their reduction: Thesis of the Doctor of Engineering: Kolomna, 1983. - 371 p.
38. *Yelbayev E.P.* On the problem of the nature of the movement of the wheelset in the curved sections of the railway track / Kharkov Polytechnic. in-t. - Kharkov, 1989. - 25 p. Dep. in VNITI No. 499.
39. Study of the influence of operating conditions and the state of the undercarriage on the wear of the ridges of non-pedestal bogies of freight diesel locomotives; Research report / VNITI; No. I-4786. - Kolomna, 1986. - 89 p.
40. *Kalker I.I., Pater A.D. dr.* Review of the theory of the local slide in the area of elastic contact with dry friction // Applied Mechanics. - M., 1971. - vol. 7. - Print 5. - p. 9-20.
41. *Carslow G., Jaeger D.* Thermal conductivity of solids. M.: Science, 1964. - 487 p.
42. *Kashura A.L., Golubenko A.L., Gorbunov N.I.* On the question of modeling the connection between a wheel and a rail with a point-to-point contact // Bulletin of the East Ukrainian national university - Luhansk: VUGU. Transport series, -1996. – p. 71-74.
43. *Kashura A.L., Golubenko A.L., Gorbunov N.I., Kostyukevich A.I.* Modeling the connection between the wheel and the rail with point-to-point contact / Problems of the development of locomotive building / Abstracts. report International scientific and technical conf., - Kyiv, 1995. - p. 3.
44. *KovalyovN.A.* Free movement of a two-axle carriage with Coulomb friction between the wheel and the rail. Vestnik VNIIZhT. - 1957. - No. 4. - p. 93-97.
45. *Kostyukevich A.I.* Numerical and experimental identification of the process of adhesion of locomotive wheels to rails: Thesis ... Ph.D. In Engineering: - Luhansk, 1991. - 232 p.
46. *Kravchuk A.S.* A variational method for solving the contact problems: Abstract of thesis. dis. ... Dr. Phys.-Math. sciences. - M., 1980. - 32 p.
47. *Kramar N.M.* Lateral horizontal vibrations of a locomotive on rubberized wheelsets: Thesis ... Ph.D. In Engineering: 05.22.07. - Voroshilovgrad, 1983 - 215 p.
48. *Krettek O.* Modern achievements in the study of the problem of adhesion // World Railways. - 1974. - No. 10. - p. 3-16.
49. *Krylov A.N.* The rocking of the ship. - M., 1951. - v. XI. - 250 p.

50. *Luzhnov Yu.M., Popov V.A., Studentsova V.F.* Energy losses and their role in the implementation of wheel-rail adhesion // Friction, wear and lubricants: Rep. Intern. Scientific and technical conference. Tashkent, May 1985 - M., 1985. - Vol. 1. - p. 133-138.
51. *Lvov N.V.* Impact of some parameters of the mechanical part of the EPS on generation of the tractive force: Thesis ... Ph.D. In Engineering: - M., 1979. - 154 p.
52. Mathematical modeling of oscillations of rail vehicles / *Ushkalov V.F., Reznikov L.M., Ikkol V.S., Trubitskaya E.Yu., Redko S.F., Zaleskiy A.I.* / eds. V.F. Ushkalov - Kyiv: Naukova Dumka, 1982, 240 p.
53. *Matsur M.A.* On the stability of motion of a four-axle passenger car with independent wheel rotation // Proceedings of the DIIT. - 1975. - Print 158. - p.68-73.
54. *Medvedev N.F., Volkov G.N.* Influence of rolling of wheelset tires on traction properties of electric locomotives. Vestnik VNIIZhT. -1966. -No. 7. -S.36-39.
55. *Meyer B.* Locomotives with high traction and coupling qualities with adjustable creep // World Railways. - 1989. No. 5. - p.18-25.
56. Mechanical part of the traction rolling stock: A textbook for higher educational institutions of the railway transport / *I. V. Biryukov, A. N. Savoskin, G. P. Burchak et al* / / eds. I.V. Biryukov. - M.: Transport, 1992. - 440 p.
57. *Mossakovsky V.I.* On the rolling of a wheelset / Izv. Academy of Sciences of the USSR. Engineering Sciences - 1957. No. 11. - p. 169-172.
58. *Nekrasov A.O., Muginstein L.A., Khatskelevich A.A., Andreyev A.V.* Patterns of dynamic distribution of the loads between traction motors / Vestnik VNIIZhT. - 1992. - N2. - p. 38-42.
59. *Osenin Yu.I.* Predicting and managing the characteristics of wheel-to-rail adhesion / K.: “VIPOL”, 1993. - 100 p.
60. *Pavlenko A.P.* Impact of the type and parameters of the traction drive on the stability the locomotive motion along the straight sections of the track // Thesis report conf. "Problems of railway transport mechanics: Enhancing the reliability and improving the design of the rolling stock”. - Dnepropetrovsk. - 1984. - p. 86.
61. *Pavlenko A.P.* Influence of dynamic processes in the traction drive on the stability of the locomotive motion // Trudy RIIZhTa. - Rostov-on-Don, 1984. - Print 1976. - p. 3-10.
62. *Pavlenko A.P.* Dynamics of the traction drives of mainline locomotives. - M.: Mechanical engineering, 1991. - 192 p.
63. *S.V. Pokrovsky* Impact of the rigidity of traction characteristics on the efficiency of using the potential coupling of electric locomotives / Vestnik VNIIZHT. - 1992. - No. 1. - p. 42-46.
64. *Popov V.A.* Influence of frictional processes on the implementation of adhesion of locomotive wheels to rails: Abstract of thesis. dis. … Ph.D. In Engineering. - M., 1985. - 24 p.
65. Development of locomotive traction / eds. *N.A. Fufryanskiy and A.N. Bevzenko* - M.: Transport, 1982. - 303 p.
66. Operating modes of mainline electric locomotives / *O. A. Nekrasov, A. L. Lisitsyn, L. A. Muginstein, V. I. Rakhmaninov* / eds. O. A. Nekrasov. M.: Transport, 1983. - 231 p.
67. *Summe G.V.* Regularities of the friction force of the wheel-rail contact in the locomotive traction mode: Abstract of thesis. dis…. Dr. tech. sciences. - M., 1986. - 286 p.

68. System for determining wheel loads // World Railways. - 1995. - No. 11. – p. 27-30.
69. Comparative dynamic tests of locomotives 2TE116A-001 and 2TE116-517; R&D Report / PKTI; OIP 2-82. - Voroshilovgrad, 1982. - 65 p.
70. *Tkachenko V.P.* Traction qualities of a locomotive with rubberized wheelsets: Thesis ... Ph.D. In Engineering: 05.22.07 Voroshilovgrad, 1983. - 216 p.
71. *Ushkalov V.F., Malysheva N.Yu.* Influence of the choice of the creep model on the joint spatial oscillations of the rail vehicle and the elastic-dissipative inertial track // Oscillations and dynamic qualities of railway rolling stock. - Dnepropetrovsk, 1989.p.10-21.
72. *Ushkalov V.F., Malysheva N.Yu.* Calculation of creep parameters in solving the problems of interaction between the wheel and the rail. Oscillations of complex mechanical systems. - K., 1990. - p. 48-58.
73. *Ushkalov V.F., Aleksandrov A.I., Kolesova E.S.* Creep model under different conditions of wheel and rail interaction // Vestnik VNIIZhT. - 1988. - No. 4. - p. 31-34.
74. *Vogel W.* Study of a method for implementing increased adhesion by traction rolling stock // World Railways. - 1992. - N9. - p. 19-25.
75. *Frederich F.* Adhesion tests carried out on the Wadgassen - Hartagen line // World Railways. 1973. - N12.
76. *Khusidov V.D., Petrov G.I., Strogova O.I. et al.* Mathematical and software support for calculating the dynamic properties of freight cars with various schemes of running gears. M., 1990. - 62 p. - Dep. in TSNIITEI TYAZHMASH, N 5377.
77. *Tsaryov I.V.* Studies on the selection of the profile of the tire and the characteristics of the connections for the locomotive crew: Thesis ... Ph.D. In Engineering: Voroshilovgrad, 1982. - 233 p.
78. *Tsaryov I.V.* Study of the influence of the geometry of the tire profile and the characteristics of elastic-dissipative connections on the horizontal dynamics of a locomotive: Abstract of thesis. dis. ... Ph.D. In Engineering. - Bryansk, 1982. - 13 p.
79. *Shannon R.* Simulation of systems. - M.: Mir, 1978. - 420 p.
80. Electrically propelled vehicles with asynchronous traction engines / *Rotanov N.A., Kurbasov A.S., Bykov Yu.G., Bykov, V.V. Litovchenko.* / eds. N.A. Rotanov - M.: Transport, 1991. - 336 p.
81. *V. V. Yakushev* Study of the forces of interaction between the wheel and the rail and taking them into account in the problems of lateral vibrations of the car: Thesis ... Ph.D. In Engineering: Bryansk, 1976. - 214 p.
82. *V. V. Yakushev* On the problem of the relationship between the longitudinal and transverse forces of the creep // Problems of the mechanics of railway transport. - Dnepropetrovsk, 1984. - p. 93.
83. *Carter F.W.* On the action of the locomotive driving wheel. - Proc.Roy.Soc. A. 1928,121, p. 151-157.
84. *Chartet A.* La Theorie Statique de Derailment d'un Essieu-Revue generale les chemins de fer, 1950, v. 69, pp. 57-63.
85. *Frederich F.* Beitrag zur Untersuchung der Kraftschubbeanspruchungen an schragrollenden Schienenfahrzeugradern. Dr.-Ing. dissertation, Berlin, 1969. - 89s.
86. *Fromm H.* Calculation of the slipping in the case of rolling deformable bars. - Zeitschrift fur angewandte Mathematik und Mechanik, 1927, B. 7, N1.

87. *Kalker JJ* Survey of Wheel-Rail Rolling Contact Theory. - Vehicle System Dynamics, 1979, v8, N 4, p.317-379.
88. *Koffman IL* Gummigefederte Lokomotivrader. - DET, 1974, 22, Nr1, s.27-30.
89. *Kojanagi S.* The stability of Motion on the Independently-Rotating-Wheel-Axle // Quart.Repts.Railway Techn.Res. Inst. - 1971. - 12. No. 1. - p. 29-33.
90. *Levi R.* Etude relative en contact des rouse sur le rail // Rev. gen. chemins de fer. - 1935. - No. 54. - p. 81-109.
91. *Luca M.* de. Un modello matematico per lo studio della stabilita di marcia transversale dei veicoli ferroviari alle alte velocita // Ing. fer. - 1969, April. - P.316-324.
92. *Meyer BR* High-adhesion locomotives with controlled creep. "Proc. Inst. Mech. Eng.: Int. Conf. Diesel Locomot. Future, York, 7-9 Apr. 1987 ". London, 1987, 209-218.
93. *Oraszvary L.,* Szilagyi G. Szabadon gordulo vasuti kerekpar mozgasanak Virsgalata // Evsk. 1990 / Vasuti Tud. kut. intez.
94. *Pater de. A.D.* The Geometrical Contact between Track and Wheelset. Vehicle System Dynamics, 17, N3, 1988. - p.127-140.
95. *Polach O.* Adhezni sily ve styku kola s kolejnici pri dynamicky promennych parametrech. Zeleznicni technika, p. 5, 1988, str. 234-237.
96. Dynamic analysis of railway wheelsets and complete vehicle systems / uang Yaung. - Delft: Delft University of Technology, Faculty for Mechanical Engineering and Marine Technology, 1993. - 156 p.

SCIENTIFIC PUBLICATION

Monograph

PREDICTION OF TRACTIVE AND DYNAMIC PERFORMANCE OF LOCOMOTIVES BY SIMULATION MODELING

Authors:

Mykola Ivanovych GORBUNOV,
Maksym Volodymyrovych KOVTANETS,
Oksana Viktorivna SERHIIENKO,
Tatiana Mykolaevna KOVTANETS
Volodymyr Serhiyovych NOZHENKO

Authorized for printing 06.12.2021.
Print format 60x84 1/16. Printing paper. Times Font.
Offset printing. Printer's sheet 5.7. Publisher's sheet 7.2.
Run of 50 copies. Issue No. 5425. Order No. 17. Contracted price.

The V. Dahl East Ukrainian National University Press

Address of the publishing house: 93400, Severodonetsk, Luhansk region.
59a Central avenue, main building
telephone: +38 (050) 218 04 78, fax (06452) 4 03 42
E-mail: vidavnictvosnu.ua@gmail.com